5-1-2002

Study of aberrations of stepper lenses in-situ using phase shifting point diffraction interferometry

P. Venkataraman

STUDY OF ABERRATIONS OF STEPPER LENSES IN-SITU USING PHASE SHIFTING POINT DIFFRACTION INTERFEROMETRY

By

P. Venkataraman
M.S. Physics
University of Cincinnati
(1996)

A thesis submitted in partial fulfillment of the
requirements for the degree of Masters in Science
in the Chester F. Carlson Center for Imaging Science
of the College of Science
Rochester Institute of technology
May 2002

Signature of the Author_____

Accepted by_____ 11/1/2002

Dr. Harvey Rhody, Coordinator, Graduate Degree Program Date

CHESTER F. CARLSON
CENTER FOR IMAGING SCIENCE
COLLEGE OF SCIENCE
ROCHESTER INSTITUTE OF TECHNOLOGY
ROCHESTER, NEW YORK

CERTIFICATE OF APPROVAL

MS DEGREE THESIS

The Masters Degree Thesis of P.Venkataraman
has been examined and approved by the
thesis committee as satisfactory for the
thesis requirements for the
Master of Science degree

Dr. Bruce W. Smith, Thesis Advisor

Dr. Zoran Ninkov, Committee Member

Paul Michaloski, Committee Member

THESIS RELEASE PERMISSION
ROCHESTER INSTITUTE OF TECHNOLOGY
COLLEGE OF SCIENCE
CHESTER F. CARLSON
CENTER FOR IMAGING SCIENCE

Title of Thesis: Study of aberrations of stepper lenses in-situ using phase shifting point diffraction interferometry

I, P. Venkataraman, hereby grant permission to the Wallace Memorial Library of R.I.T. to reproduce my thesis in whole or in part. Any reproduction will not be for commercial use or profit.

Signature: _____

Date: 8/16/2002

STUDY OF ABERRATIONS OF STEPPER LENSES IN-SITU USING PHASE SHIFTING POINT DIFFRACTION INTEROMETRY

by
P.Venkataraman

submitted to the
Chester F. Carlson
Center for Imaging Science
College of Science
in partial fulfillment of the requirements
for the Master of Science Degree
at Rochester Institute of Technology

ABSTRACT

Stepper lenses are tested by the lens manufacturer using various interferometric methods like phase measurement interferometry (PMI), before they are assembled onto the stepper or scanner. Once the system is set up, there are a few methods to study the lens aberrations *in-situ* using interferometry. The methods currently used are direct ones like direct aerial image measurement (DAIM) or indirect ones in which images of lines and spaces are formed in the photoresist and the aberrations inferred from scanning electron microscope (SEM) images of these. We propose using phase shifting point diffraction interferometry (PSPDI) for the purpose of measuring aberrations *in-situ*. The method has the advantages of being simple, and of having relaxed coherence length requirements and applicability over a wide wavelength range. We present results from a prototype experiment done on a 436 nm optic on an optical bench using a 442 nm He-Cd laser as source.

ACKNOWLEDGEMENTS

I would like to thank Dr. Bruce Smith for all his advice and help. I thank the committee members for their patience and help. I would like to thank Hoyoung Kang and Dr. Ralph Schleif for their discussions, Lena Zavyalova, Tolic Bourov, Suraj Bhaskaran for their help with mask and, coating. I would like to thank all the staff at Center for Imaging Science and Microelectronic Engineering Department for their help.

TABLE OF CONTENTS

LIST OF TABLES

LIST OF FIGURES

1. Introduction

The International Technology Roadmap for Semiconductors (ITRS) (Table 1) [1] gives requirements for key lithographic capabilities such as resolution, total overlay, chip size, defect density, mask size, and field size. Lithographic lenses used in steppers play a very important role in defining the limits to which optical lithography can be taken as they determine most the ITRS requirements. By design, the performance of these lenses is near diffraction limited. Resolution that can be obtained by optical lithography for a projection stepper is given by [30]:

$$W = \frac{k_1 \lambda}{NA} \tag{1.1}$$

Where k_1 (typical values are 0.25 to 0.8) is a constant depending on various process parameters, λ is the illumination wavelength (typical values 365nm(Hg arc lamp), 248nm(KrF excimer laser), 193nm(ArF excimer laser), and NA is the image side numerical aperture (typical values from 0.28 to 0.8). As can be seen from the equation we can get better resolution by reducing the wavelength or increasing the NA or by doing both. That is exactly what the lens manufacturers are doing. The downside of this is that the usable depth of focus (DOF) is reduced as is evident from the equation [30]:

$$DOF = \frac{k_2 \lambda}{NA^2} \tag{1.2}$$

Where k_2 is also a constant depending on process parameters (typical values are 0.8 to 1.0). As the resolution limit decreases, the performance of lenses becomes more critical.

The lens manufacturer or lithography tool manufacturer tests the lenses, during and after the assembly of the lens. This is done by, through the lens (TTL)[2] interferometry methods like phase measurement interferometry (PMI)[3], direct aerial image measurement (DAIM)[3], point spread function measurement (PSF)[4], and opto-electromechanical ray trace [5].

Year	1998	2001	2004	2007	2010
Technology Generation (μm)	.25	.18	.13	.10	.07
DRAM (bits)	256 M	1 G	4 G	16 G	64 G
Development capability (min feature size (μm)	.16	.11	.08	.05	.03
Minimum feature size (um)					
Isolated lines	.24	.16	.11	.08	.05
Dense lines	.25	.18	.13	.10	.07
Microprocessor chip size (mm^2)	300	360	430	520	620
Field size (mm^2)	484	1250	1250	1250	1250
Defect density, lithography only @ defect size (μm)	320 .08	135 .06	60 .04	30 .04	15 .02
Mask size (inches), quartz	6 by 6	9 by 9	9 by 9	9 by 9	9 by 9

Table 1: Technology roadmap for lithography [1].

Once the lithography tool is in the shop floor, indirect methods like focal surface (FOCAL)[3], scanning electron microscope (SEM)[3] analysis of images formed in the resist, 3-beam interference [6], In-situ interferometer by Litel [33] are used to evaluate the performance of the stepper as a whole. PMI uses a piezo-mounted mirror on one arm of Twymann-Green interferometer to introduce some known phase shift. The wavefront

phase error is extracted from the interference patterns obtained at each phase shift of the mirror. In DAIM, aerial images of isolated spaces and dense line patterns are magnified and imaged on to a CCD array at multiple height positions in the neighborhood of Gaussian focus, and the images analyzed for aberrations. In FOCAL, the focal surface of the wavefront is measured by imaging isolated lines onto a thin resist using the optical alignment system and inferring the focal plane variation over the whole field. In the PSF method, the point spread function is measured through focus and across the field and the point spread function is used to evaluate image quality. In 3-beam interference method, imaging condition of a fine grating by 3-beam interference is used to quantify coma, astigmatism, and spherical aberrations. In opto-electromechanical ray trace, the image is analyzed ray-by-ray using a small mechanically moved aperture to measure the ray aberration and from these get the wave aberration.

With the lens performance becoming more critical it would be advantageous if the lithographer had a means of measuring the aberrations of the lens in-situ by a simple and accurate method, so that he/she can use the stepper optimally to suit every situation. Towards this end we propose using Phase shifting point diffraction interferometry to measure the aberrations of stepper lenses in-situ. The reasons for choosing this method is because it is easy to implement, low on hardware requirements, applicable over a wide range of wavelengths, is accurate enough to measure the aberrations one would expect in a stepper.

2. Background

This chapter gives a brief introduction on aberrations, optical lithography, image metrics, and effects of aberrations on imaging.

2.1 Aberrations

Aberrations or errors in image formation can be described in terms of either ray, or wave aberrations. Aberration is indicated by the failure of all rays emanating from a single object point to intersect at a single image point after passing through the optics. The coordinate offset of rays in the image surface indicates the magnitude of ray aberration [7], [8]. Aberrations can also be expressed as the failure of the path from entrance pupil coordinates to exit pupil coordinates to be the same for rays emanating from the same object point. The path difference between the actual wavefront and a perfect wavefront at the exit pupil plane represent wave aberrations.

The relation between wave and ray aberration is that ray displacement error can be expressed as the derivative of wavefront error in terms of pupil coordinates. In Figure 2.1.1, P_0'P_0" represents ray aberration, QQ' represents wave aberration. Figure 2.1.1 is for on-axis case.

$$(x_i, y_i) = R / n_i * (\partial W / \partial x, \partial W / \partial y) \qquad (2.1.1)$$

Where (x_i, y_i) are coordinates of P_0" with respect to P_0', and R is the distance between exit pupil plane and the image plane, n_i is the refractive index on the image side, W represents wave aberration, and (x, y) are the exit pupil coordinates.

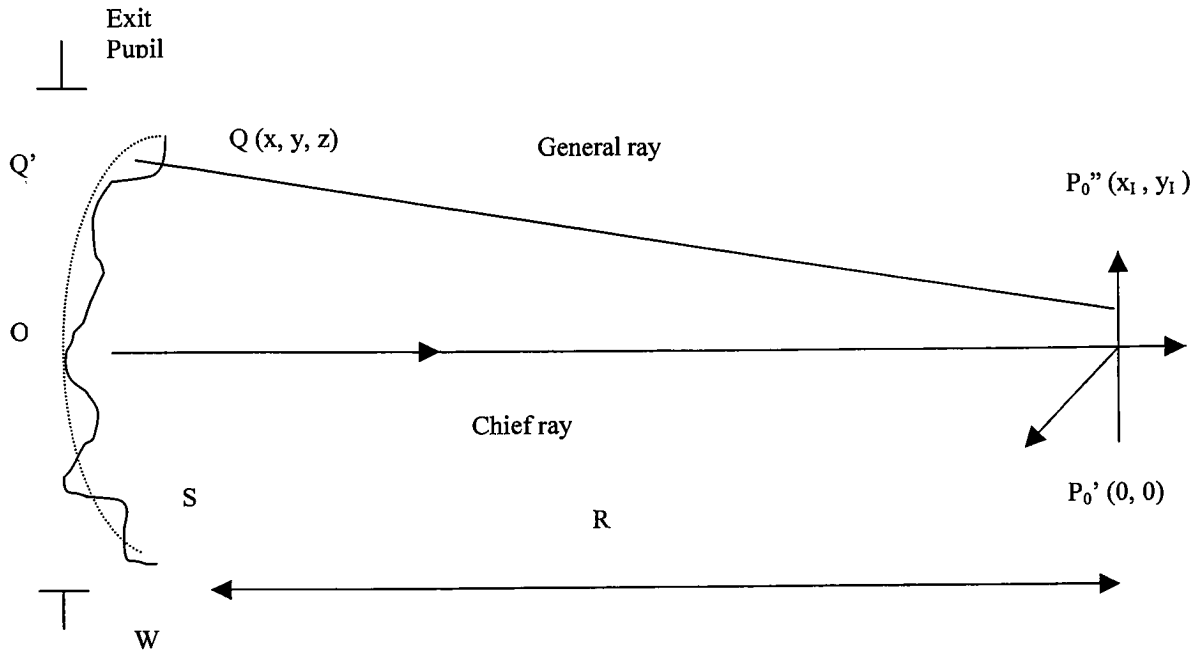

Figure 2.1.1 Aberrated wavefront for an on-axis point object.

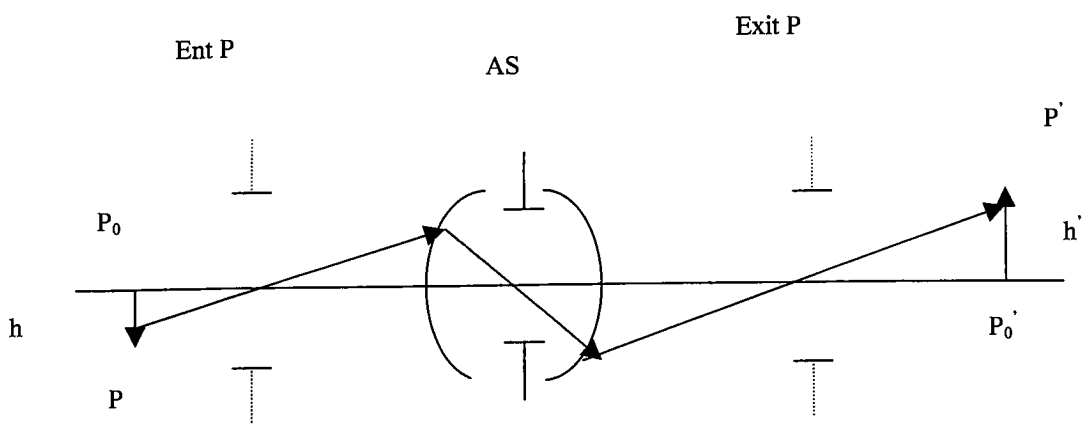

Figure 2.1.2 Schematic of an optical imaging system.

One mostly encounters rotationally symmetric optical systems like in Figure 2.1.2. The wave aberration can be expressed as a power series in terms of object/image (h) and pupil (r) coordinates:

$$W(\bar{h};\bar{r}) = \sum_{l=0}^{\infty}\sum_{p=0}^{\infty}\sum_{m=0}^{\infty} c_{lpm} h^{2l+m} r^{2p+m} \cos^m(\theta - \theta_0) \qquad (2.1.2)$$

Where degree of each term of the series in object and pupil coordinates is always even (2*(l+m+n)). We can remove the explicit dependence on image height by suppressing it and also writing pupil coordinates as $\rho = r/a$, where 'a' is the maximum radius of the exit plane pupil, θ is the azimuthal angle in the pupil plane, we get:

$$W(\rho,\theta) = \sum_{n=1}^{\infty}\sum_{m=0}^{n} a_{nm}\rho^n \cos^m\theta \qquad (2.1.3)$$

$$\text{Where } a_{nm} = a^n \sum_{l=0}^{\infty}(2l+m)h'^{2l+m} \qquad (2.1.4)$$

The above is usually written as a sum of mutually orthogonal polynomials called Zernike polynomials. These are given by:

$$W(\rho,\theta) = \sum_{n=0}^{\infty}\sum_{m=0}^{n} c_{nm}[2(n+1)/(1+\partial_{m0})]^{1/2} R_n^m(\rho)\cos m\theta \qquad (2.1.5)$$

Where c_{nm} are the expansion coefficients which depend on the image height h', and n and m are positive integers including zero and n-m>=0.

$$R_n^m(\rho) = \sum_{s=0}^{(n-m)/2} \frac{(-1)^s (n-s)!}{s!(n+m/2-s)!(n-m/2-s)!} \rho^{n-2s} \tag{2.1.6}$$

is the radial polynomial of degree n in ρ.

The orthogonality of the radial polynomial and the angular function are given by:

$$\int_0^1 R_n^m(\rho) R_{n'}^m(\rho) \rho d\rho = \frac{1}{2(n+1)} \delta_{nn'} \tag{2.1.7}$$

and

$$\int_0^{2\pi} \cos m\vartheta \cos m'\vartheta d\vartheta = \pi(1+\delta_{m0})\delta_{mm'} \tag{2.1.8}$$

The expansion coefficients are:

$$c_{nm} = (1/\pi)[2(n+1)(1+\delta_{m0})]^{1/2} \int_0^1 \int_0^{2\pi} W(\rho,\vartheta) R_n^m(\rho) \cos m\vartheta \rho d\rho d\vartheta \tag{2.1.9}$$

Using the above expressions one can calculate the variance of the aberration function:

$$\sigma_w^2 = \sum_{n=1}^{\infty} \sum_{m=0}^{n} c_{nm}^2 \tag{2.1.10}$$

An example of some Zernike polynomials with the aberration they represent is shown in Table 2.1.1. Figure 2.1.3 shows some of the aberration plots.

Term (n,m)	Fringe Zernike Polynomial	Common Name
1(0,0)	1	Piston
2(1,1)	$R\cos(\alpha)$	X Tilt
3(1,1)	$R\sin(\alpha)$	Y Tilt
4(2,0)	$2R^2-1$	Power
5(2,2)	$R^2\cos(2\alpha)$	3rd Order Astigmatism
6(2,2)	$R^2\sin(2\alpha)$	3rd Order 45^0 Astigmatism
7(3,1)	$(3R^3-2R)\cos(\alpha)$	3rd Order X Coma
8(3,1)	$(3R^3-2R)\sin(\alpha)$	3rd Order Y Coma
9(4,0)	$(6R^4-6R^2+1)$	3rd Order Spherical
10(3,3)	$R^3\cos(3\alpha)$	3rd Order 3-Point
11(3,3)	$R^3\sin(3\alpha)$	3rd Order 45^0 3-Point
12(4,2)	$(4R^4-3R^2)\cos(2\alpha)$	5th Order Astigmatism
13(4,2)	$(4R^4-3R^2)\sin(2\alpha)$	5th Order 45^0 Astigmatism
14(5,1)	$(10R^5-12R^3+3R)\cos(\alpha)$	5th Order X Coma
15(5,1)	$(10R^5-12R^3+3R)\sin(\alpha)$	5th Order Y Coma
16(6,0)	$20R^6-30R^4+12R^2-1$	5th Order Spherical
17(4,4)	$R^4\cos(4\alpha)$	3rd Order 4-Point
18(4,4)	$R^4\sin(4\alpha)$	3rd Order 45^0 4-Point
19(5,3)	$(5R^5-4R^3)\cos(3\alpha)$	5th Order 3-Point
20(5,3)	$(5R^5-4R^3)\sin(3\alpha)$	5th Order 45^0 3-Point
21(6,2)	$(15R^6-20R^4+6R^2)\cos(2\alpha)$	7th Order Astigmatism
22(6,2)	$(15R^6-20R^4+6R^2)\sin(2\alpha)$	7th Order 45^0 Astigmatism
23(7,1)	$(35R^7-60R^5+30R^3-4R)\cos(\alpha)$	7th Order X Coma
24(7,1)	$(35R^7-60R^5+30R^3-4R)\sin(\alpha)$	7th Order Y Coma
25(8,0)	$70R^8-140R^6+90R^4-20R^2+1$	7th Order Spherical
26(5,5)	$R^5\cos(5\alpha)$	3rd Order 5-Point
27(5,5)	$R^5\sin(5\alpha)$	3rd Order 45^0 5-Point
28(6,4)	$(6R^6-5R^4)\cos(4\alpha)$	5th Order 4-Point
29(6,4)	$(6R^6-5R^4)\sin(4\alpha)$	5th Order 45^0 4-Point
30(7,3)	$(21R^7-30R^5+10R^3)\cos(3\alpha)$	7th Order 3-Point
31(7,3)	$(21R^7-30R^5+10R^3)\sin(3\alpha)$	7th Order 45^0 3-Point
32(8,2)	$(56R^8-105R^6+60R^4-10R^2)\cos(2\alpha)$	9th Order Astigmatism
33(8,2)	$(56R^8-105R^6+60R^4-10R^2)\sin(2\alpha)$	9th Order 45^0 Astigmatism
34(9,1)	$(126R^9-280R^7+210R^5-60R^3+5R)\cos(\alpha)$	9th Order X Coma
35(9,1)	$(126R^9-280R^7+210R^5-60R^3+5R)\sin(\alpha)$	9th Order Y Coma
36(10,0)	$252R^{10}-630R^8+560R^6-210R^4+30R^2-1$	9th Order spherical
37(12,0)	$924R^{12}-272R^{10}+3150R^8-1680R^6+420R^4-42R^2+1$	11th Order Spherical

Table 2.2.2: Zernike polynomials and the aberrations they represent.

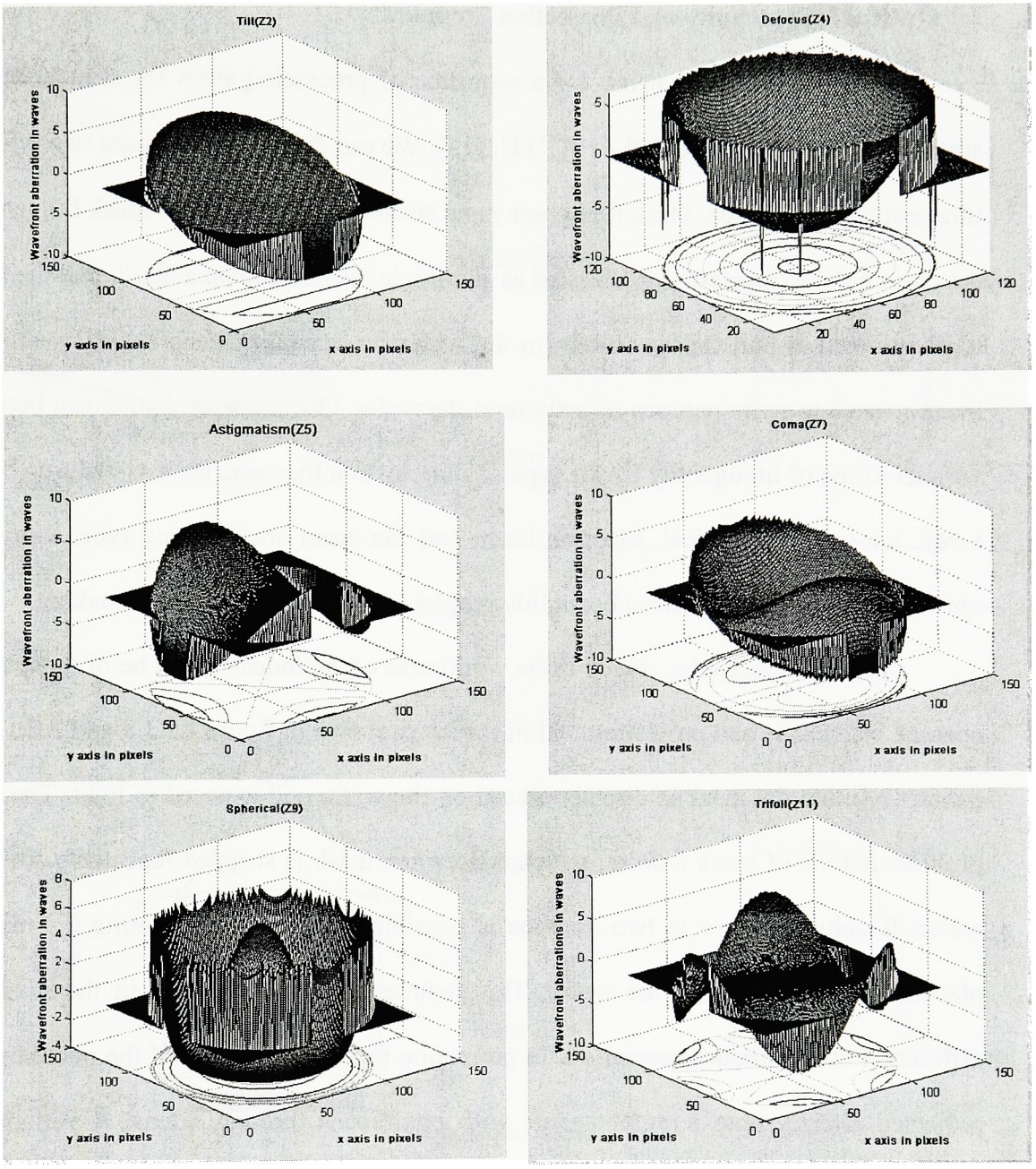

Figure 2.1.3: Some typical wavefront plots showing different types of aberrations.

2.2 Optical Lithography and Projection Steppers

Lithography is the name for a sequence of processing steps for structuring the surface of planar substrates [9], [10], [11], [12]. We can distinguish between two types of lithographic procedures. Mask lithography and scanning lithography. In mask lithography the pattern to be transferred is encoded as amplitude distribution on a mask, and the mask is illuminated to transfer the pattern to the wafer. In scanning lithography a modulated beam is used to write patterns directly onto the wafer. One can also distinguish between various forms of lithography by the type of illumination they use, such as electron beam, x-ray, ion-beam, or optical. Electron beam and ion-beam are scanning type, x-ray and optical are mask type. Electron beam lithography is usually used for mask making.

Optical lithography, which is the workhorse of the industry, can be of three types, contact, proximity, and projection. All of these are shown in figure 2.2.1.a and 2.2.1.b. In contact printing the mask is directly placed on the wafer and exposed to light. The main problem here is of mask defects, which arise when mask is stripped repeatedly from the wafer. Resolution down to two microns is possible. In proximity printing the mask is placed a little away from the wafer. This reduces the wear and tear in the mask but diffraction effects reduce resolution. In projection printing an image of the photomask is projected directly onto a wafer coated with photoresist through a lens. A variation of above is scanning or step and repeat projection in which a portion of the mask is imaged onto the wafer and the exposure repeated by either scanning or stepping over the entire wafer.

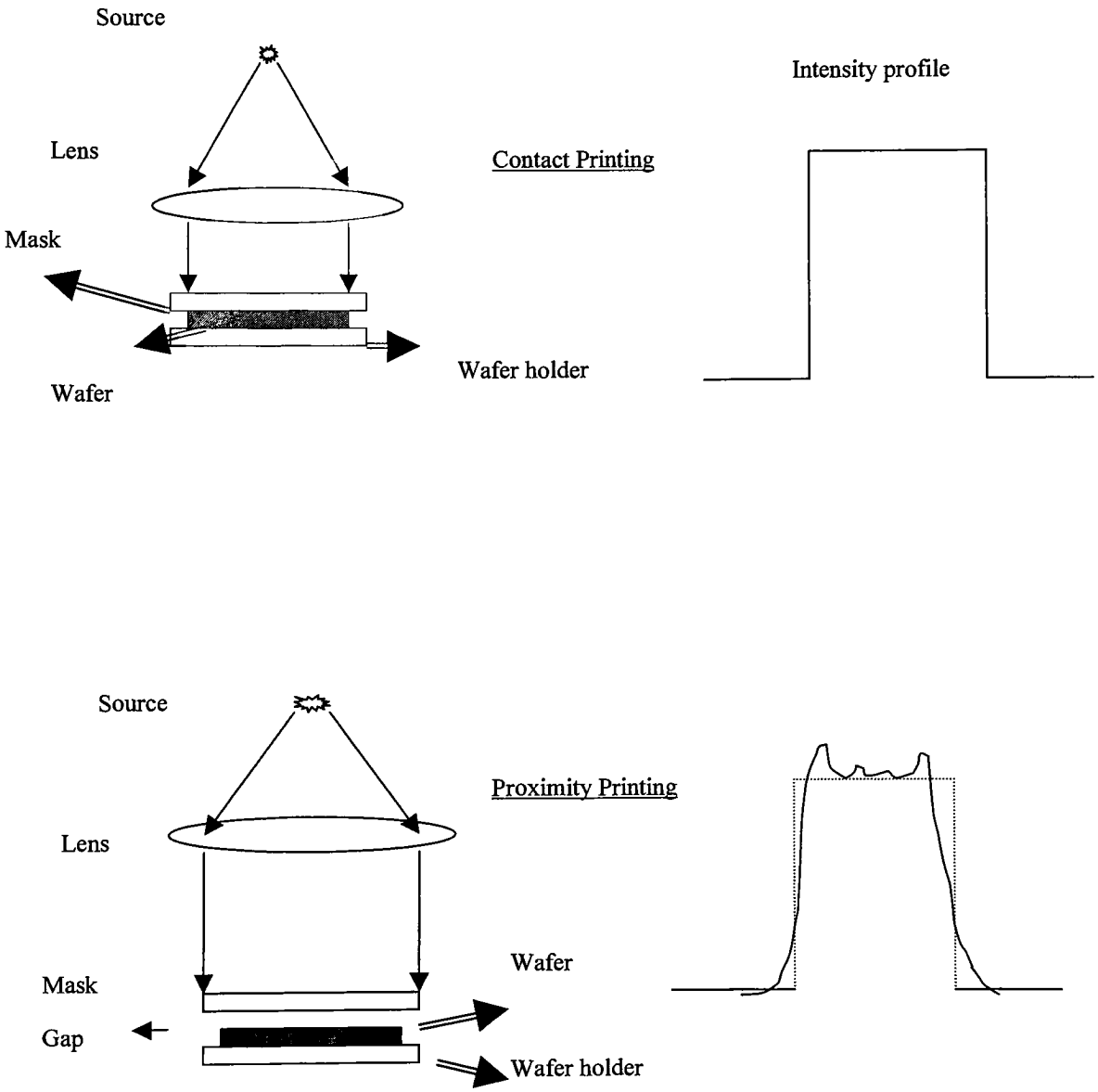

Figure 2.2.1.a: Optical lithography contact and proximity printers.

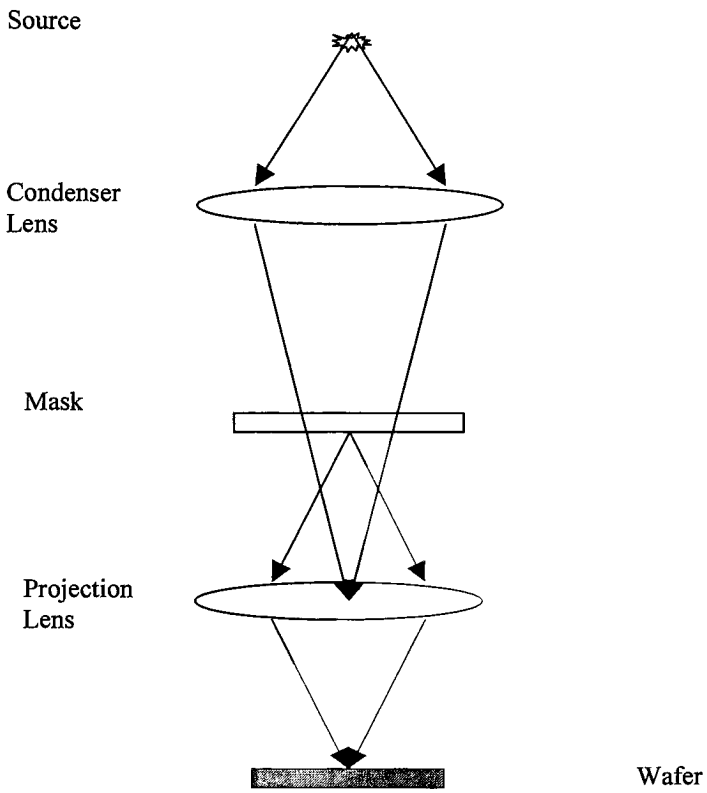

Figure 2.2.1.b: Optical lithography projection printer.

The basic components of a projection stepper are 1) illumination system 2) lens 3) mask holder 4) wafer holder and 5) alignment system.

1) *Illumination system*: An example of the two extreme cases, coherent and incoherent illumination is shown in Figure 2.2.2. In new steppers available now one can change the coherence factor. Usually a Kohler type illumination is used [30]. The technique of focusing the illumination source in the entrance pupil of the image forming optics is called Kohler illumination. This ensures uniform illumination over the field.
2) *Projection lenses*: The lenses used for projection are some of the best made and have near diffraction- limited performance. Projection lenses have become more complicated with higher demands placed on them. A list of some of the lenses being, and to be used in IC manufacturing is shown in Table 2.2.1. The lenses are usually telecentric. The exit pupil of a telecentric lithography lens is located at infinity, this implies that each point on the wafer is illuminated with a cone of light whose axis is perpendicular to the wafer surface.
3) *Mask holder*: It is basically a stage for holding the mask. The stage can be moved in 'x' and 'y' directions, where the optic axis of the system is along 'z' axis. The mask holder holds the mask in the object plane of the projection lens.

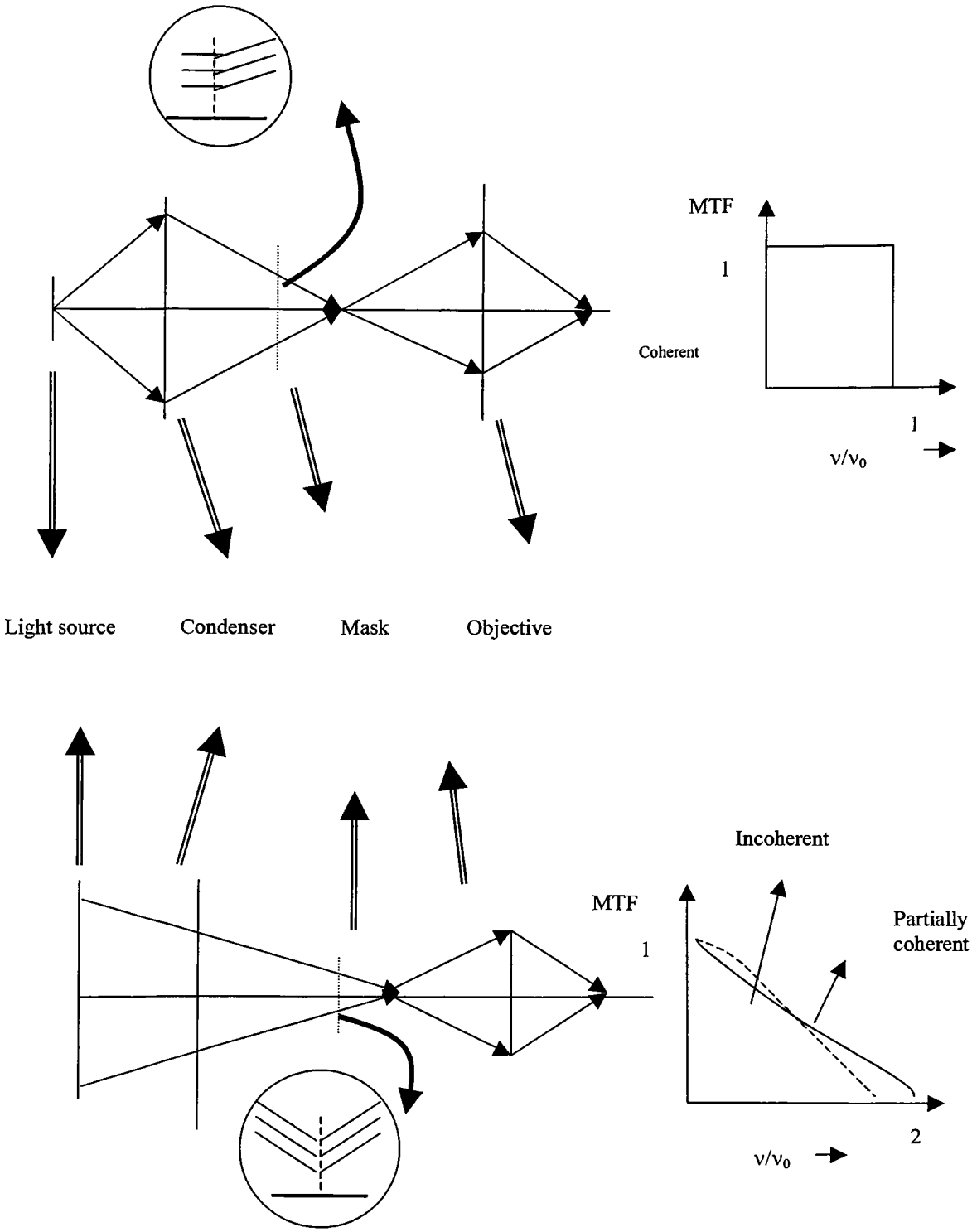

Figure 2.2.2 Coherent and incoherent illumination, ν is the spatial frequency and ν_0 is the cutoff spatial frequency [9].

Minimum feature in microns	NA	λ (nm)	k_1	Resolution in microns	Depth of Focus (DOF) in microns
1	.38	436	.8	.92	3.02
.7	.4	365	.75	.7	2.28
.5	.48	365	.6	.46	1.58
.35	.6	365	.5	.35	1.01
.25	.6	248	.6	.25	.69
.18	.6	193	.5	.17	.54

Table 2.2.1: Microlithographic lenses for IC production [1].

4) *Wafer holder*: This is a stage to hold the wafer in place using vacuum, while it is exposed. This stage has the freedom to be moved along all the 3 axes.

5) *Alignment system*: Usually uses interferometric techniques to align the mask and the wafer. Also helps the wafer holder to be moved accurately while scanning or stepping.

2.3 Image Metrics

The performance of a stepper lens can be measured or specified in the following ways:

1) Resolution:

$$W = \frac{k_1 \lambda}{NA} \tag{2.3.1}$$

where k_1 is a constant, which depends on process parameters, λ is source wavelength and NA the Numerical Aperture of the lens.

This equation explains the trend for lower wavelength and higher NA lenses. The resolution possible for various lenses is shown in Table 2.2.1

2) Depth of Focus (DOF):

$$DOF = \frac{k_2 \lambda}{NA^2} \tag{2.3.2}$$

where k_2 is a constant, which depends on process parameters. The depth of focus values for various lenses is given in Table 2.2.1. DOF reduces when one lowers wavelength, or increases NA.

3) *Modulation transfer function (MTF)* [30]. This is the ratio of contrast in image to that in object, as function of spatial frequency. Given by:

$$MTF(\nu) = (2/\pi)[Cos^{-1}(\nu/\nu_0) - \nu/\nu_0(1-(\nu/\nu_0)^2)^{1/2}] \tag{2.3.3}$$

Where $\nu_0 = 2NA/\lambda$ for incoherent illumination and $\nu_0 = NA/\lambda$ for coherent illumination.

MTF for partially coherent illumination is given by:

$$MTF_P(\sigma,\nu) = G(\sigma,\nu)MTF(\nu) \tag{2.3.4}$$

Where

$$G(\sigma,\nu) = \frac{1}{1-\frac{4}{\pi}\sin(\frac{\nu\lambda}{2NA})} \; for \nu < \nu_1$$

$$= \frac{1-\frac{4}{\pi}\sin(\frac{\nu_2\lambda}{2NA})\frac{(\nu-\nu_1)}{(\nu-\nu_2)}}{1-\frac{4}{\pi}\sin(\frac{\nu\lambda}{2NA})} \; for \nu_1 < \nu < \nu_2 \tag{2.3.5}$$

$$< 1 for \nu_2 < \nu$$

$$where \nu_1 = (1-\sigma)\frac{NA}{\lambda} and \nu_2 = (1+.18\sigma)\frac{NA}{\lambda}$$

σ is the degree of coherence given by:

$$\sigma = \frac{NA_c}{NA_o} \tag{2.3.6}$$

Where NA_c is Numerical Aperture of condenser lens, NA_o is the Numerical Aperture of the objective.

The MTF Plots for the three kinds of illumination is shown in Figure 2.2.2.

4) *Strehl ratio (SR)*: This is the ratio of image intensity affected by aberrations to that of the image intensity without any aberrations.

A common method to quantify the amount of aberration in a lens is to specify the root-mean square (RMS) deviation of the wavefront aberration. For fringe Zernikes this is equal to the weighted sum of the aberration coefficients, given as

$$RMS^2(\bar{R}) = \sum_m (c_m(\bar{R})\varepsilon_m)^2 \tag{2.3.7}$$

Where $\varepsilon_m = k/2(n+1)$, n is the order of the radial polynomial, k is 1 for non-rotationally symmetric, and 2 for rotationally symmetric polynomial. One can get the Strehl ratio (SR) from RMS using:

$$SR(\bar{R}) = e^{-[k_0 RMS(\bar{R})]^2} \tag{2.3.8}$$

where $k_0 = 2*\pi/\lambda$, λ is wavelength.

5) NILS (Normalized Image Log Slope) [1]

$$\text{Given by: } NILS = L\frac{1}{E_0}\frac{\partial E}{\partial x} \tag{2.3.9}$$

where E_0 is average exposure dose and L is the linewidth.

Fractional change in line width is related to fractional change in exposure dose by:

$$\frac{\Delta L}{L} = 2(NILS)^{-1}\frac{\Delta E}{E} \tag{2.3.10}$$

This implies that as NILS decreases so does exposure latitude. This does not uniquely determine optical contribution to process latitude, because it depends on print bias too. An example of NILS is shown in Figure 2.3.1.

6) Process Window

This is a plot of usable depth of focus as a function of exposure dose. The presence of aberrations reduces this window so it is a useful way to determine the stepper performance. An example of process window simulated using Prolith (a commercial

software for lithography modeling) is shown in Figure 2.3.2 for a 365 nm stepper with lens having an NA of 0.5 for coherent illumination for an iso line 500 nm wide.

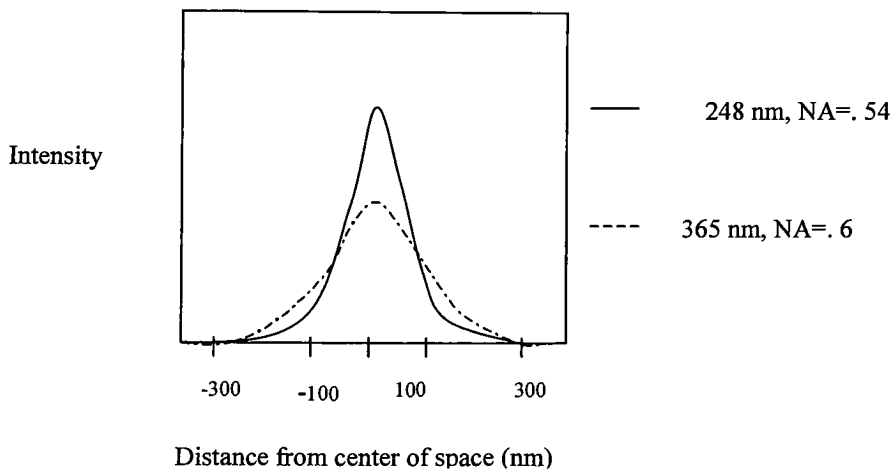

Figure 2.3.1a: Light intensity distribution of a 350nm isolated (iso) space at best focus.

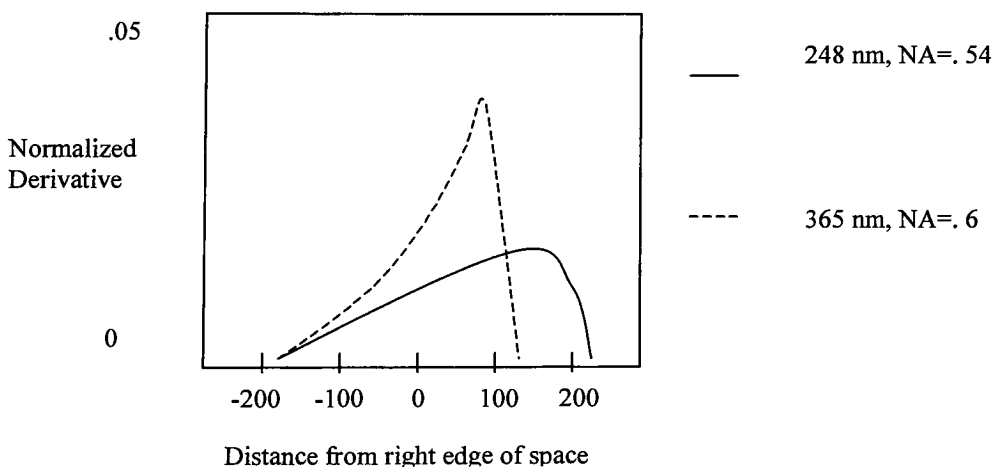

Figure 2.3.1.b: Normalized derivative of the light intensity distribution. Normalized derivative is in units of μm [30]. As seen above NILS value at the edge is nearly doubled by lowering the exposure wavelength. This translates to increase in exposure latitude and linewidth control.

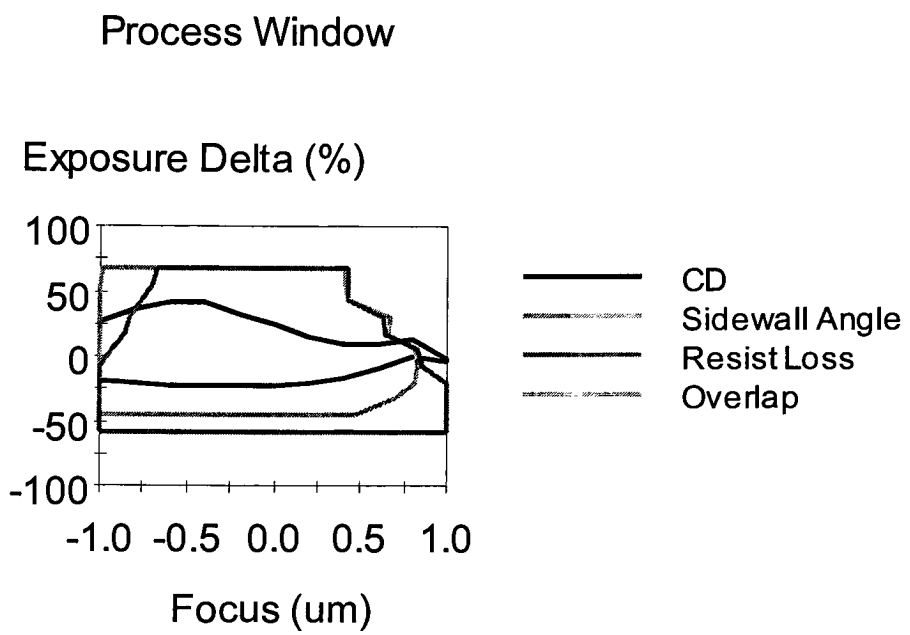

Figure 2.3.2: Process Window for 365 nm, .5 NA stepper with coherent illumination for a 500 nm isolated(iso) line. These plots indicate usable exposure and focus latitude w.r.t parameters like Critical Dimension(CD), Sidewall Angle(Profile of the step), and Resist Loss. In the regions inside the shown inside the contours the parameters are within acceptable limits. The overlap of all these shows the usable exposure and focus latitude with which all these parameters are within acceptable limits.

2.4 Effect of aberrations on lithographic images.

The relation between the image in the film at image plane and wave aberrations can be written as [13]

$$I(x,y,z) = \int\int d\alpha_0 d\beta_0 J(\alpha_0,\beta_0) \mid E(x,y,z:\alpha_0,\beta_0) \mid^2 \qquad (2.4.1)$$

Where E the electric field at the image plane and can be written as

$$E(x,y,z:\alpha_0,\beta_0) = FT^{-1}\{\bar{O}(\alpha-\alpha_0,\beta-\beta_0)P(\alpha,\beta)F(\alpha,\beta:z)e^{ik_0 z_0}e^{ik_0 W(\alpha,\beta)} \qquad (2.4.2)$$

Where FT^{-1} is the inverse Fourier Transform, J (α_0,β_0) is the effective source distribution in the projection lens entrance pupil with area S. O (α-α_0,β-β_0) is the shifted Fourier transform of the object. P (α,β) is the projection lens transmission function. F (α,β: z) is the thin film contribution within the photoresist to a depth of 'z'. $e^{ikz\gamma}$ is the focus phase term. $e^{ikW(\alpha,\beta)}$ is the contribution due to the wave aberration. Here $k_0 = 2*\pi/\lambda$, λ is the wavelength of illumination. Using the above equation or slightly modified versions of it the effect of individual aberrations have been modeled by inputting individual aberration terms in the wavefront term W(α,β) (The individual Zernike terms are shown in Table 2.2.2).

Looking at the aberrations term by term, the following generalizations can be made [14]: -

The piston term Z_1 indicates constant phase over the aperture and does not affect imagery.

Z_2 and Z_3 represent tilt of the Optical Path Difference (OPD) wavefront, and the effect on imaging is a positional shift of the image in x or y direction on the image plane. This shift can be represented as a vector proportional to the Zernike coefficients. This can be seen in Figure 2.4.1 where the aerial image of a 500 nm isolated (iso) line is shown for a 365 nm, 0.5 NA stepper, with no aberrations, and with 0.05 waves of x coma aberration.

Z_4 represents defocus. OPD surface is quadratic, and it degrades image contrast, edge slope, pattern fidelity, and resolution. Z_5 and Z_6 represent astigmatism. OPD is saddle shaped, and shifts orthogonal lines positively and negatively. For Z_6 the shift is for horizontal and vertical lines, for Z_5 the orthogonal lines are now oriented at +- 45^0. Z_7 and Z_8 represent coma and image contribution from different pupil radii shift relative to one another. Z_{10} and Z_{11} represent three clover. OPD has 3-fold symmetry and causes undesirable imaging artifacts. Z_9 represents third order spherical. OPD is 3^{rd} order surface and the focus shift across the image varies with ρ. This effect is shown in Figure 2.4.1.

The effect of aberrations can be inferred in many ways.

1) Aerial Image: Aerial image is affected by aberrations and can be simulated using the equation 2.4.1 shown early in the section. Figure 2.4.1 shows simulation done using Prolith for a 500 nm iso-line on 365 nm, 0.5 NA stepper illuminated with coherent illumination.

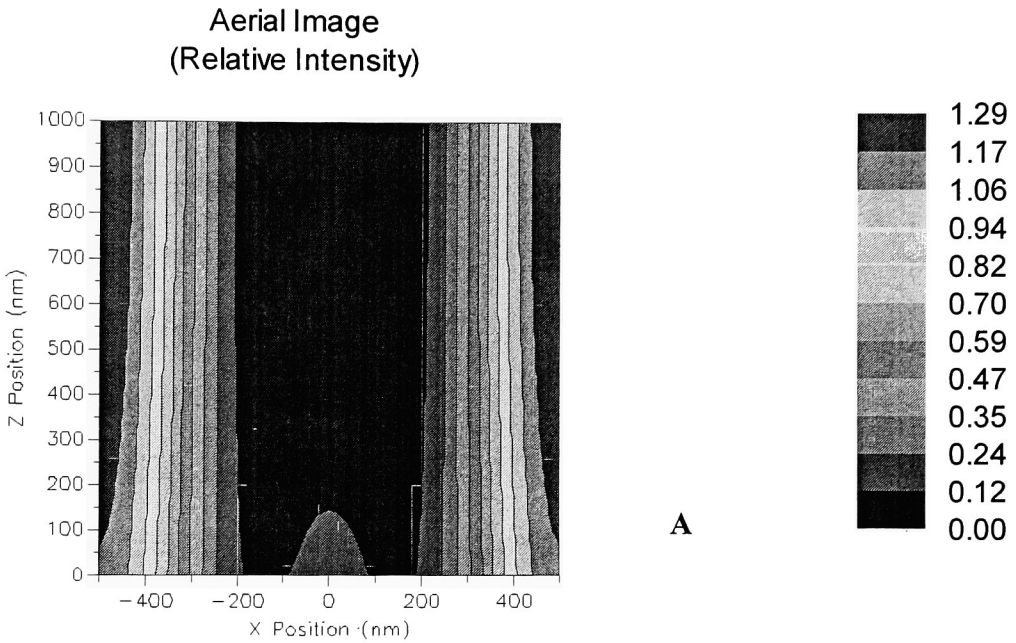

Figure 2.4.1: Aerial image of a 500nm iso line imaged by a 365 nm, 0.5 NA stepper. A- without aberrations, B- with 0.05 waves of coma aberration, C- with 0.05 wave of spherical aberration. These plots show the relative intensity at different focus positions. A slice parallel to x-axis at a z position will indicate intensity variation along x at that z location.

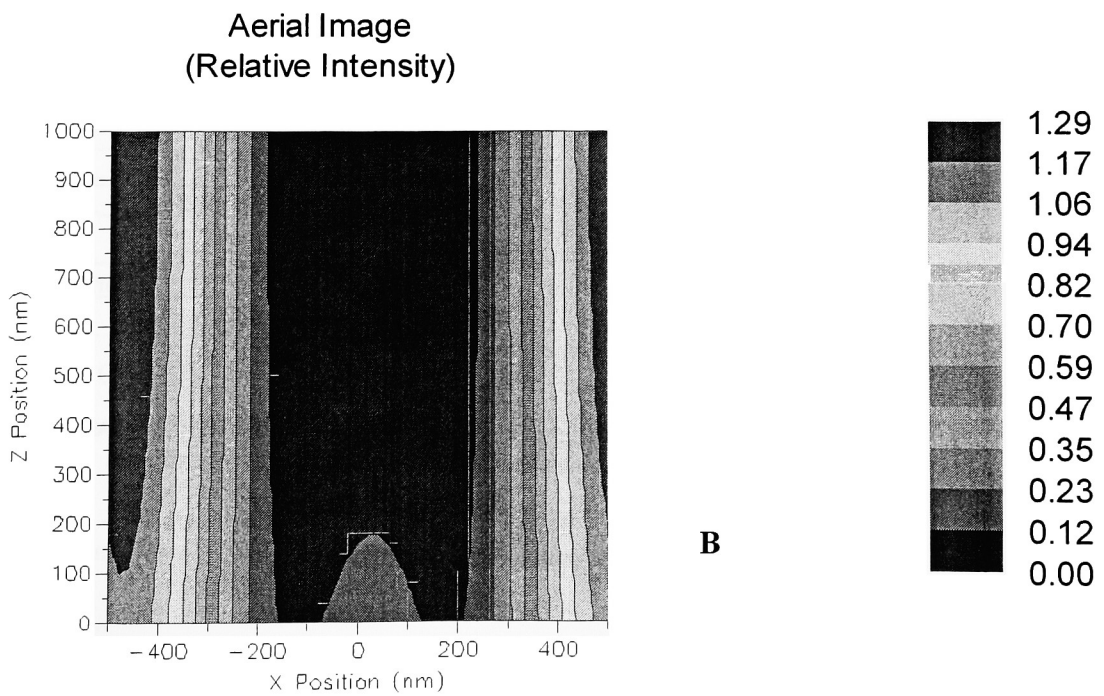

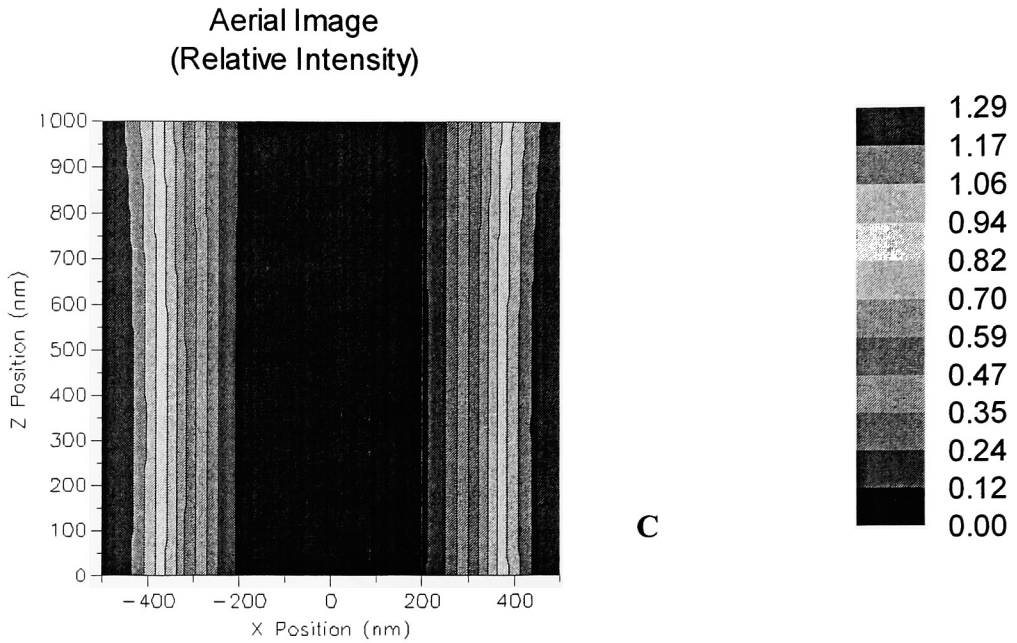

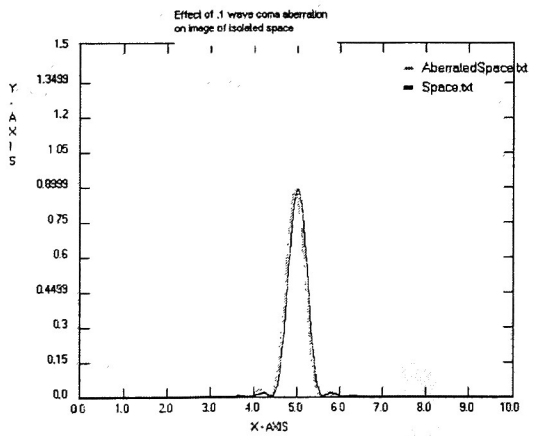

A

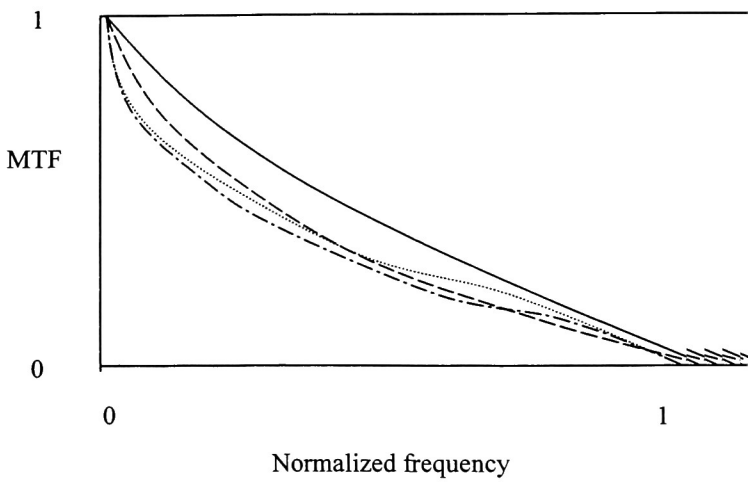

B

Figure 2.4.2: The first figure A shows PSF without, and with .1 waves of coma aberration. The second figure B shows variation MTF with various aberrations.

In B —— is for no aberration, -·-·- is for spherical aberration, - - - is for coma aberration, ····· Is for defocus aberration. The aberration value is 0.07 waves in each case.

2) *MTF or PSF*: Aberrations change the MTF characteristic of a lens. One can also look at the change in PSF. MTF and PSF are Fourier Transform pairs of each other [32]. An example of non-aberrated PSF and MTF, along with PSF and MTF for an optic with 0.1 waves of coma aberration are shown in Figure 2.4.2. When aberrations are less than $\lambda/14$ RMS, the shape of the central core of the PSF is essentially unchanged except for a decrease in peak intensity.

3) *Process Window:* The effect of aberrations can also be seen as a reduction in process window. This is shown in Figure 2.4.3 where Process Window for a 365 nm, .5 NA stepper is shown with 0.05 waves of coma, 0.05 waves of spherical, and no aberrations for the cases of coherent and partially coherent illumination (σ=0.5).

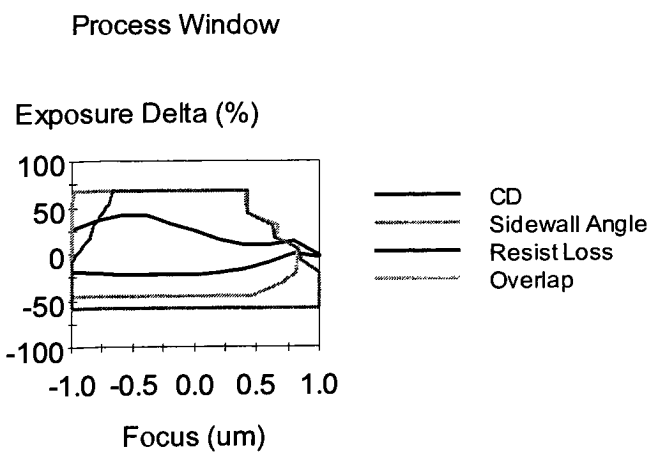

(A)With no aberration. Coherent illumination

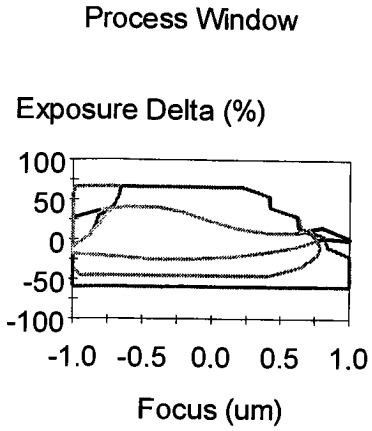

(B) With 0.05 waves of spherical aberration. Coherent illumination

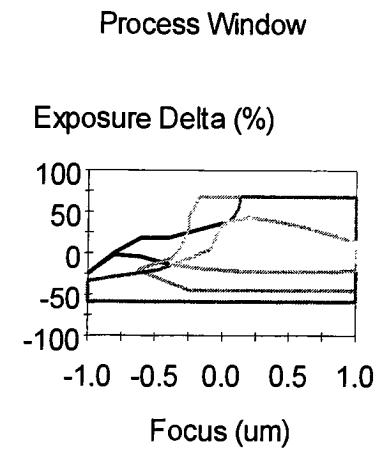

(C) With 0.05 waves of Coma. Coherent

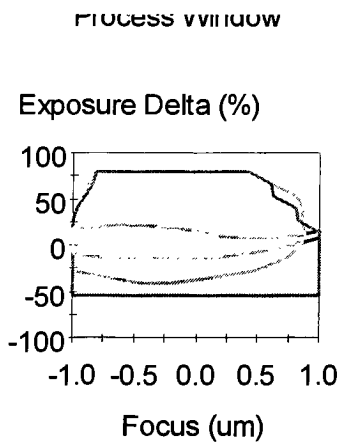

(D) With no aberrations. Partially coherent illumination

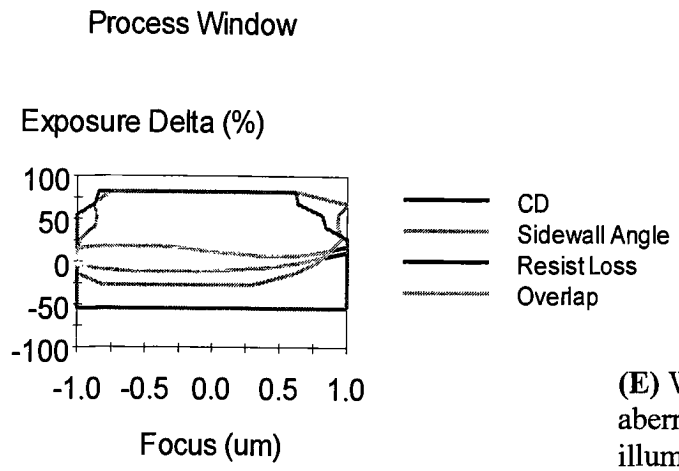

(E) With 0.05 waves of spherical aberration. Partially coherent illumination

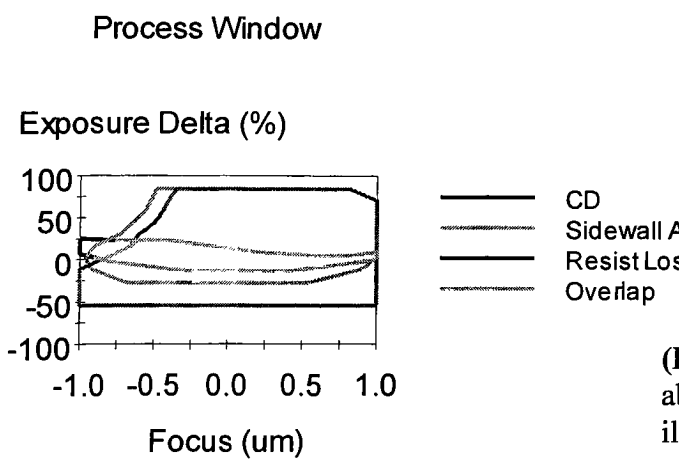

(F) With 0.05 waves of coma aberration. Partially coherent illumination.

Figure 2.4.3: All the above shown simulations were done on Prolith for a 365 nm, 0.5 NA stepper imaging an iso line. A, B, C are for coherent illumination, D, E, F are for partially coherent illumination for σ=.5. As can be seen aberrations reduce both usable depth of focus and exposure latitude.

3) *Strehl's Ratio:* The following results shown in Figure 2.4.4 are from a simulation done at IBM [31], the optical system considered is a 257 nm, .35 NA lens with partially coherent illumination (σ=0. 6). In each case the aberration value is 0.02 waves. The following indicate combinations chosen. a) Spherical+ is Z11+Z22+Z37, b) Spherical- is Z11-Z22+Z37, c) Coma+ is Z7+Z16+Z29, d) Coma- is Z7-Z16+Z29, e) Astigmatism+ is Z5+Z12+Z23, f) Astigmatism- is Z5-Z12+Z23, g) Combination+ is Z5+Z7+Z11+Z12+Z16+Z22+Z23+Z37, h) Combination- is Z5+Z7-Z11-Z12-Z16+Z22+Z23+Z37. Z's indicate Zernike coefficients (The individual Zernike terms are shown in Table 2.2.2).

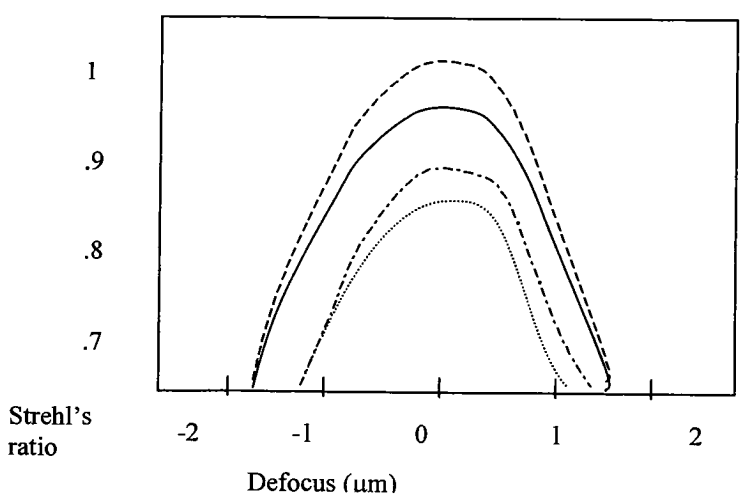

Figure 2.3: Strehl's ratio through focus for various aberrations.
No aberrations ----
a, b, c, d, e, f ——
g - - - -
h .....

3 Experimental Procedures

In this chapter the experimental procedure used is explained.

3.1 Phase shifting point diffraction interferometry.

In point diffraction interferomtry [15] a beam diffracted from a pinhole in the object plane falls on the test optic and the beam after passing through the optic passes through a partially transmitting screen with a sub-resolution pinhole in it as shown in Figure 3.1.1. The sub-resolution pinhole diffracts a reference beam and this interferes with the transmitted beam to form an interference pattern. For accurate analysis of the static fringe pattern, a significant number of tilt fringes need to be introduced by displacement of the reference pinhole laterally from the focus of the test optic. The light intensity getting to the sub-resolution pinhole is reduced. This with the small size of the sub-resolution pinhole necessitates reduction of the intensity of the test wave by attenuation.

This technique was modified by H Medeki, et al [16] with the possibility of introducing phase shift by using a grating. In this setup as shown in Figure 3.1.2 a small pinhole at the object plane of the optic to be tested produces a nearly spherical beam to illuminate a grating kept in between the optic and the object point. The grating pitch and the distance between the grating and object side pinhole are chosen so that more than 2 diffraction orders pass through the optic. In the image plane two of the diffraction orders are spatially filtered with a mask which has one window, and a sub resolution pinhole, separated by the an amount equal to the distance between the zeroth and the first order.

The first order beam is made to pass through the large pinhole (approximately 20 to 40 times the resolution limit of the optic) in a mask kept the image plane and is the test beam. The sub resolution pinhole allows the zeroth order beam to pass through, generating the reference beam. The reference and the test beam interfere to produce an interference pattern, which can be analyzed to get the wavefront phase error due to the test optic. The grating allows for the possibility of varying phase. By moving the grating in a direction perpendicular to both the optic axis and the direction of grating rulings by one fourth of the grating pitch, the phase of the 1st order beam changes by 90 degrees and that of the zeroth order is unaltered. This can be used to generate a set of interferograms shifted with respect to each other by 90 degrees, which in turn can be analyzed using 5-frame method [25](The method is explained in section 3.3). The accuracy of the method depends on various parameters, the most important being the quality of the reference wavefront, which in turn is dependent on the size of the sub-resolution pinhole. Other factors are the 3rd order coma error due to the geometry of the setup. This effect can be used to calibrate the interferometer. We can use a mask with two sub-resolution pinholes, and compare the experimentally calculated coma to the theoretically predicted value of coma. Another possible source of error is detector misalignment. A lot of work on PSPDI has been done by the group at the department of Electrical Engineering at University of California Berkeley, where they used the method to characterize EUV cameras [17], [18], [19], [20], [21], [22].

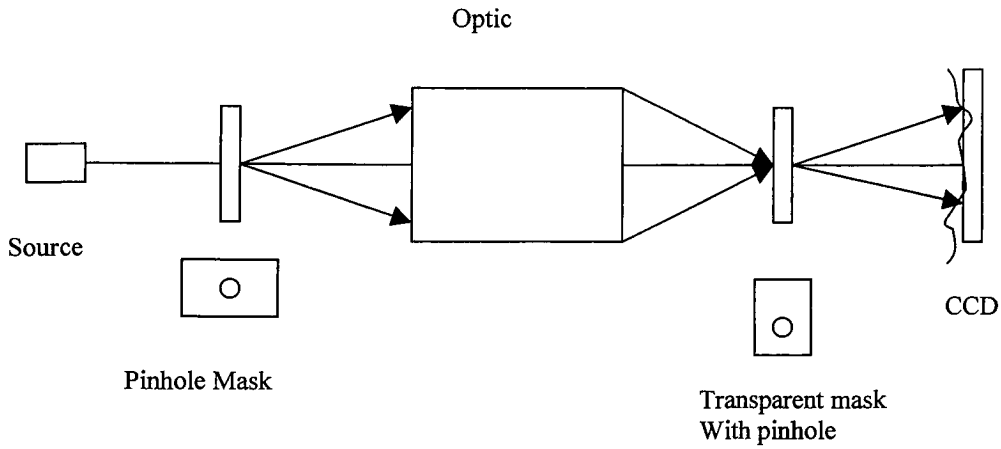

Figure 3.1.1: Point diffraction interferometry setup.

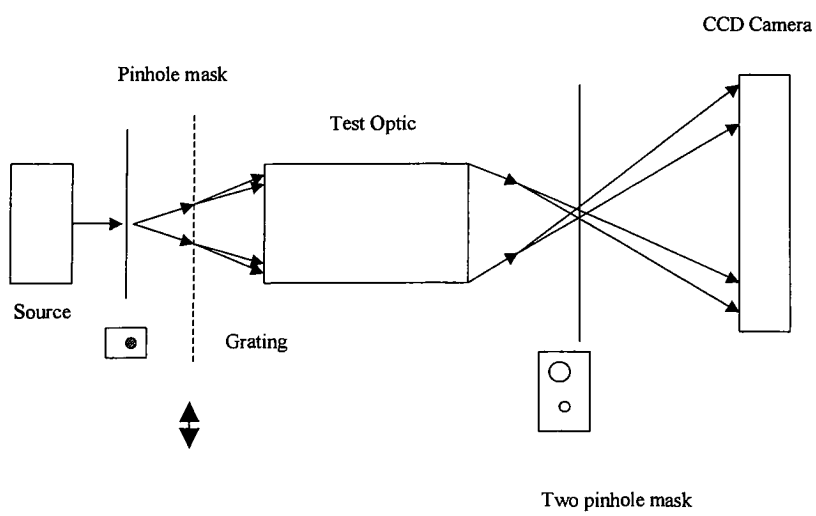

Figure 3.1.2: A schematic of PSPDI.

3.2 Error sources in the experimental set-up

3.2.1 Error due to a parallel glass plate being introduced in a converging or diverging beam of light (Figure 3.2.1).

The grating pattern and the image plane pinhole mask are both written on 0.09 inches thick chrome plated glass plates. The parallel glass plate introduces primary aberrations when they are in the path of a converging or diverging beam as is the case for the grating and pinhole mask plate [8]. These aberrations can be expressed as:

$$W(r,\theta:h) = a_s(r^4 - 4hr^3\cos\theta + 4h^2r^2\cos^2\theta + 2h^2r^2 - 4h^3r\cos\theta) \qquad (3.2.1)$$

where a_s is the coefficient of spherical aberration and is given by:

$$a_s = \frac{(n^2-1)t}{8n^3S^4} \qquad (3.2.2)$$

Let us make an order of magnitude calculation of the aberration for the grating plate. From the figure it is seen that (r/S)~NA. "n" is the refractive index of glass, "S" is the separation between glass plate and image plane, "t" is the thickness of the plate, "r" is beam diameter at the plate. The first term of equation 3.2.1 will then will be:

$$\frac{(n^2-1)tNA^4}{8n^3} \qquad (3.2.3)$$

Using this and the values, t =2286 um, NA =0.028 on the object side, n=1.5 we get W to be of the order of $6*10^{-5}$ microns, which is negligible.

On the image side the pinhole mask is aligned such that the chrome coated part of the plate faces the optic. This implies that the aberration introduced is in the interference

pattern generated between the reference and test beam. We can only reduce it by using the thinnest glass or quartz plate possible.

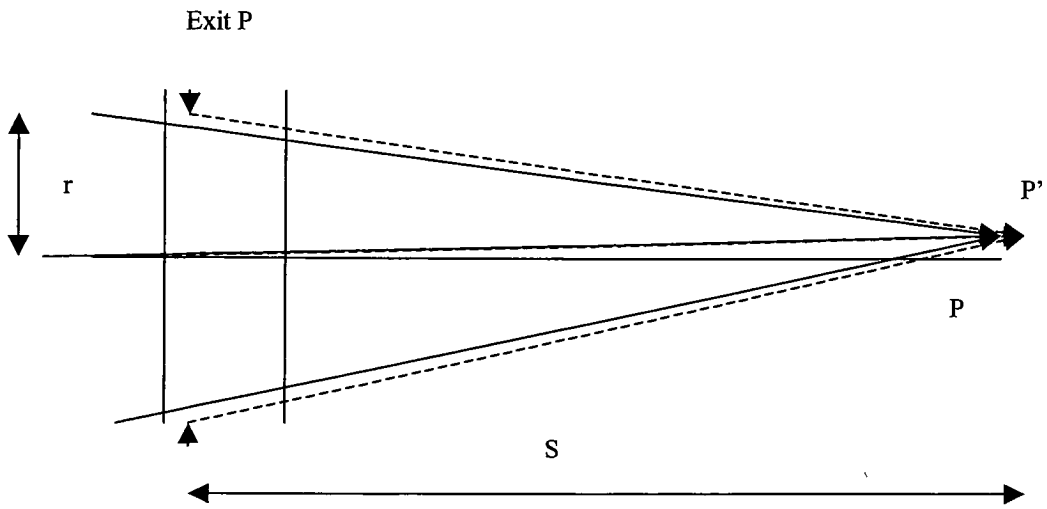

Figure 3.2.1: Parallel glass plate in a converging beam. Rays incident on plate converge to P' instead of P.

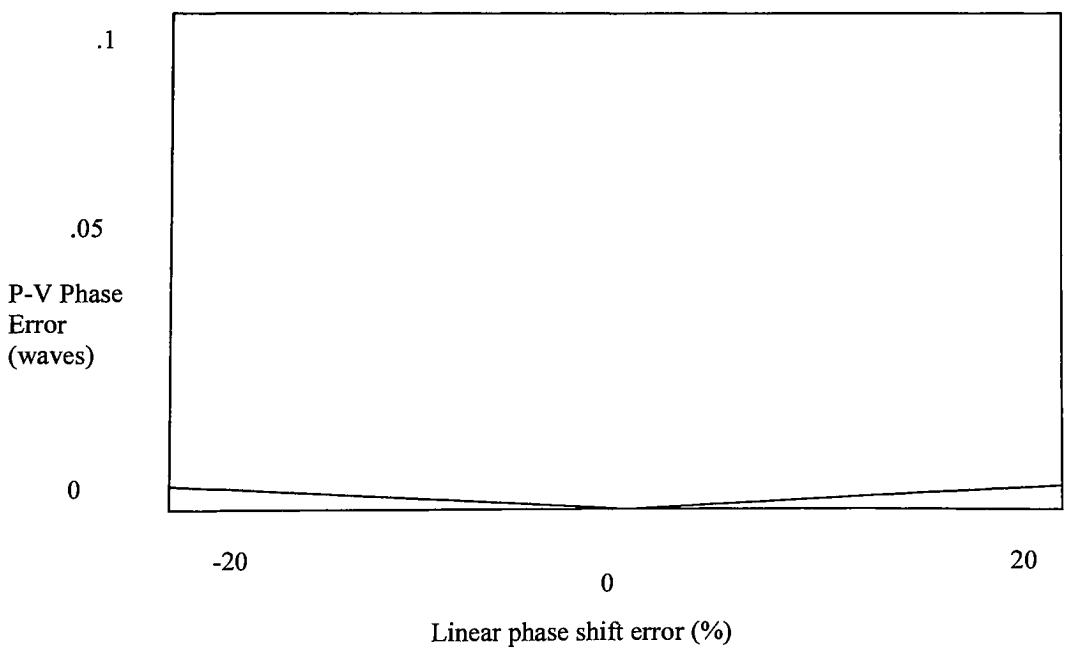

Figure 3.2.2: Measured Phase Error vs linear phase shift error of grating [25].

3.2.2 Error in calculated wavefront due to error in grating motion.

As described in section 3.1 on experimental procedure the grating needs to be moved by a value equal to one fourth that of the grating pitch. The error can be reduced, by using a large grating constant so that the required movement of grating is coarse enough. In the present set-up the grating needs to be moved by 20 microns, which is coarse enough for the stages being used with least count of 1 micron. Also as seen in figure 3.2.2 [25], the use of 5-bucket algorithm implies that the wavefront error due to error in grating motion is approximately less than 0.002 waves for errors in motion of grating up to +-5%.

3.2.3 Reference pinhole errors

As the pinhole diameter is of finite size, it allows for finite spatial frequency bandwidth to pass through. It is reasonable to assume that these errors decorrelate as a function of pinhole position relative to the point spread function of the optic. This effect can be mitigated, by an averaging process wherein pinhole position is changed by a fraction of the optic point spread function. The other source of error is defects in pinhole shape that is the holes being different from perfect circles. This can be reduced, by averaging over an ensemble of equivalent sized pinholes [24].

For this particular experiment done on the optic bench, another source of error is the non- ideal size of the reference pinhole. The ideal pinhole should be less than a

micron, and the size of the pinhole used in the measurement set-up is of 2 microns. A micron pinhole was written, but did not clear fully possibly because of wet etching done on a thick chrome layer. Modeling was done to get an idea of what errors a non-ideal pinhole would introduce. The assumption was that ideal pinhole was a delta function, and the non-ideal was a rect function twice the size of the ideal. The assumption is valid because the Fourier transform of a 1 pixel image gives the response expected from ideal delta function The far field diffraction field, which represents the wavefront at the exit pupil, was calculated for the ideal and non-ideal reference pinhole and a set of 37 Zernike polynomials fitted to the portion of difference wavefront filling an NA of 0.28. This will indicate the systematic error due to non-ideal pinhole. A first approximation to the far field wavefront diffracted from the experimental pinhole is the diffraction pattern of a coherent beam from a simple circular aperture in a planar screen based on Kirchoff's model of diffraction theory. A pinhole of diameter, d, diffracts a spherical wavefront that fills NA= $\sin\theta = 1.22\lambda/d$. The Zernike coefficients calculated for non-ideal pinhole for the 436 nm optic are shown in Figure 3.2.3. The non-ideal 2-micron under fills the NA of optic by approximately 5 percent. The calculated error wavefront has non-zero values for the aberration terms Z_9 and Z_{17}. The first of these is important as the second one can possibly be reduced or removed by Park's method [Appendix B], it being an unsymmetric aberration.

3.2.4: Systematic geometric effect of coma

Because of the inherent large tilt in the set-up there is a systematic coma error in the reconstructed wavefront [19, 21, 24]. Assuming the separation between the reference pinhole and the window to lie along x axis and expressing r_1, and r_2 (Figure 3.2.4) as a function of mixing plane position in polar coordinates (ρ,θ) and by not neglecting higher order terms we have

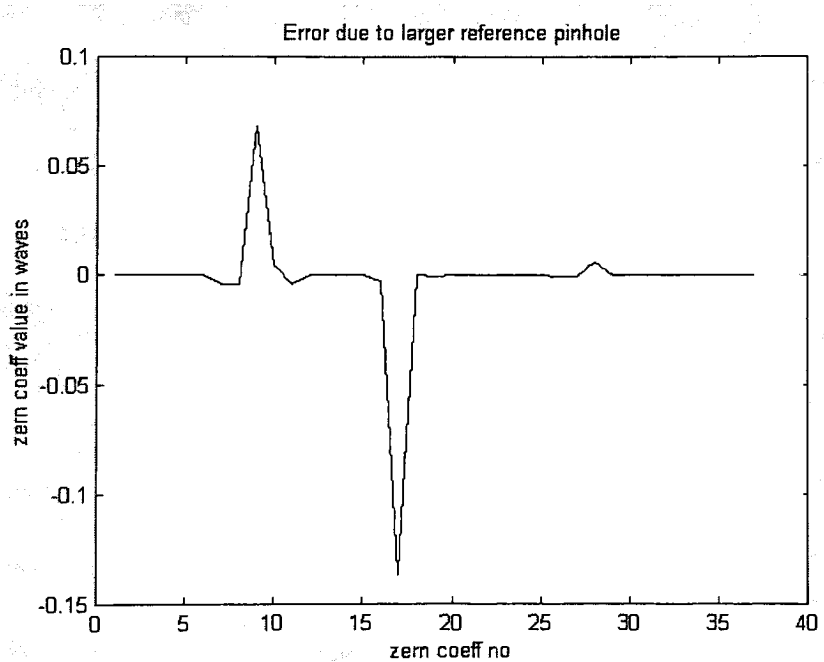

Figure 3.2.3: Error due to larger reference pinhole. The above plot shows the Zernike coefficients for the calculated difference wavefront, between the ideal sized pinhole of diameter d and the non ideal pinhole of size 2d.

$$\Delta r = r_1 - r_2 = (\frac{s}{2z^3}\rho^3 - [\frac{s}{z} - (\frac{s}{2z})^3]\rho)\cos\theta \qquad (3.2.4)$$

where s is the separation between pinholes, z is the separation between the image plane and the pinhole plane.

In terms of Zernike polynomials the above equation can be written as:

$$\Delta r = (C(3\rho^3 - 2\rho) + T\rho)\cos\theta \qquad (3.2.5)$$

Where C is the coma coefficient and T is tilt coefficient along x direction.

$$C = \frac{s}{6}(\frac{r_m}{z})^3 = \frac{s}{6}\tan^3(\sin^{-1}(NA)) \approx \frac{s}{6}(NA)^3 \qquad (3.2.6)$$

This can be used to calibrate the set-up. If we use two sub-resolution pinholes in the image plane mask, and then measure the wavefront it should yield only the tilt and systematic coma error, because now two reference beams are interfering. Comparing the calculated systematic coma with theoretical one, the set-up can be calibrated. This calibration could not been done for 436 nm optic as the 2 reference pinhole mask was not written. The values in both cases would be 1 micron for 436 nm, and .16 microns for the 248 nm.

3.2.5: Detector misalignment effect

Proper alignment needs the detector to be perpendicular to the central ray of the optical system [19, 21, 24]. If the detector is not aligned perpendicular and has an angular

tilt γ_x , and γ_y with respect to x and y-axes respectively as shown in figure 3.2.5, then the path length error due to this is given as:

$$\Delta r = \frac{s\rho^2}{2z^2}[\gamma_x(\cos 2\theta + 1) - \gamma_y \sin 2\theta] \tag{3.2.7}$$

This can be interpreted in terms of astigmatism and defocus errors and corresponding coefficients are given respectively as:

$$e_a = \frac{1}{2}NA^2(\gamma_x{}^2 + \gamma_y{}^2)^{1/2} \tag{3.2.8}$$

and

$$e_d = \frac{1}{4}\gamma_x NA^2 \tag{3.2.9}$$

where $NA=r_m/z$

The values would be 0.000154 waves (e_a), 0.000054 waves (e_d) for 436 nm per degree of tilt.

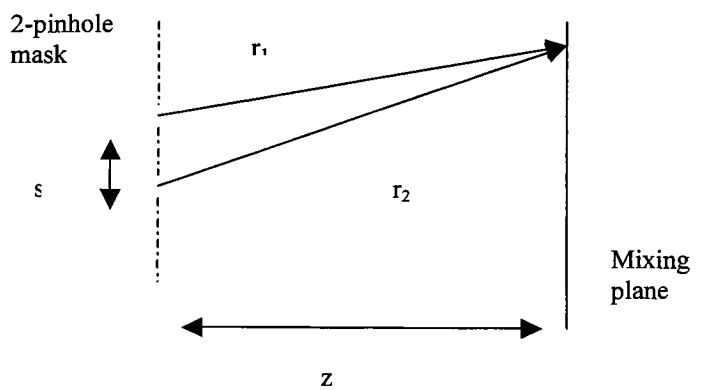

Figure 3.2.4: Systematic geometric effect of coma.

3.2.6: Error due to scattering of reference beam through the spatial window

In the present experiment the separation between the reference pinhole and the spatial window is equal to the width of the window [23]. In this case there is a possibility of reference beam being scattered through the window.

Signal reaching the detector is:

$$U(f_x) = A\partial(f_x - f_c) + rect(\frac{f_x}{W})[n(f_x) + S(f_x)]$$

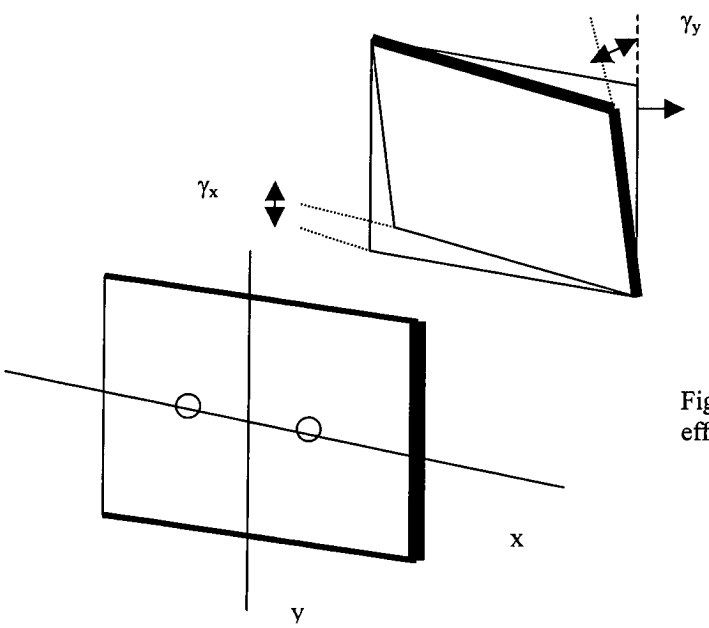

Figure 3.2.5: Detector misalignment effect.

where W is the width of the window, δ represents the pinhole, n represents the noise (scattered signal from pinhole through the window), and S represents the signal energy passing through the window. This is shown in Figure 3.2.6. This can be avoided by changing the separation to 1.5 times the width of the window in which case there is no scattering as seen in figure 3.2.6.

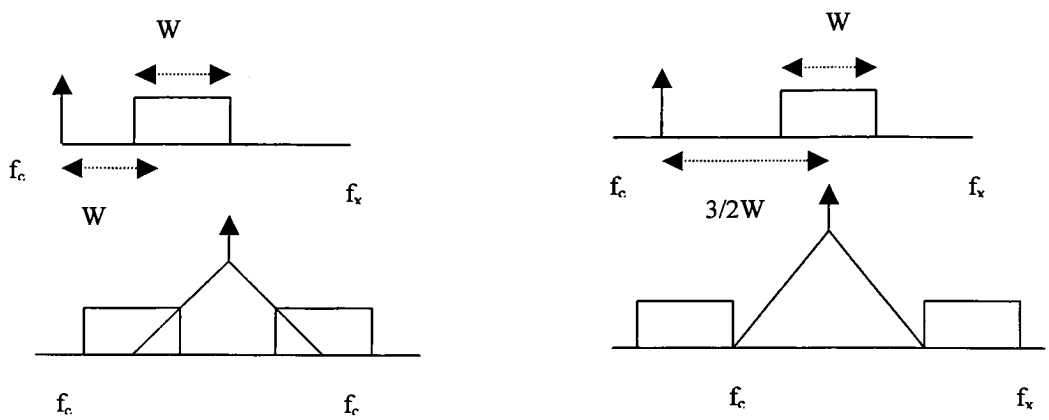

Figure 3.2.6: The top two figures show the spatial spectrum of the field in the recording plane, the bottom two figures show spatial spectrum of recorded irradiance. The figures in the left are for the case of separation between the pinhole and window equal to W the right is for separation 3/2W.

3.3 The 5-frame method.

This method can be used for any interference set-up, which has the possibility of shifting the phase of the interference pattern [23], [24], [25]. The phase shifting itself can be done in various ways. Some of the methods employed for phase shifting are a) moving mirror, in which a reference mirror is moved in a direction perpendicular to the optic axis using a piezo. b) tilted glass plate c) moving diffraction grating, in which a grating is moved in a direction perpendicular to the optic axis and the grating ruling d) Rotating Analyzer or Wave plate. If ϕ is the wavefront phase difference between the test and the reference wave then the Intensity of interference pattern recorded can be written as:

$$I = I_0(1+\gamma Cos(\phi)) \tag{3.3.1}$$

This technique uses 90^0 phase shifts to minimize phase calibration errors. This algorithm reduces the possibility of the numerator and denominator tending to zero, and thereby reduce the uncertainty in the calculation. It uses five frames of intensity with relative phase shifts of α. I_0 is the zero order intensity, γ is the contrast function.

$$\begin{aligned} I_1 &= I_0(1+\gamma Cos(\phi-2\alpha)) \\ I_2 &= I_0(1+\gamma Cos(\phi-\alpha)) \\ I_3 &= I_0(1+\gamma Cos(\phi)) \\ I_4 &= I_0(1+\gamma Cos(\phi+\alpha)) \\ I_5 &= I_0(1+\gamma Cos(\phi+2\alpha)) \end{aligned} \tag{3.3.2}$$

These equations can be combined to yield:

$$\frac{I_2 - I_4}{2I_3 - I_5 - I_1} = \frac{Sin\alpha Sin\phi}{(1 - 2Cos2\alpha)Cos\phi} \tag{3.3.3}$$

when $\alpha = \pi/2$ the equation simplifies to:

$$\phi = \tan^{-1}[\frac{2(I_2 - I_4)}{2I_3 - I_5 - I_1}] \tag{3.3.4}$$

$$\gamma = \frac{\sqrt{[2(I_2 - I_4)]^2 + (2I_3 - I_5 - I_1)^2}}{4I_0} \tag{3.3.5}$$

The phase thus inferred from the interferogram is usually wrapped in the range of 0 to 2π, due to the nature of arctangent calculation. To get the correct phase of the wavefront the phase needs to be unwrapped. There are many methods of unwrapping the phase. The basic assumption all of these methods make is that it is not possible to have a phase jump of 2π between two neighboring pixels in the phase wavefront.

3.4 Phase unwrapping:

Phase of wavefront when determined by interferometric methods is wrapped in the range of 0 to 2π, and needs to be unwrapped. See Figure 3.4.1 as an example. The simplest method of unwrapping involves a sequential scanning through of data line by line as shown in Figure 3.4.2 [26]. While scanning the line adjustment (a phase of π added or subtracted) is made to the pixel values with the assumption that phase varies smoothly and neighboring pixels cannot have a jump of more than π. At the end of each line the phase difference between the current pixel and the pixel on the line below are compared, corrected and the line scanned in the opposite direction. This implies that we are treating the 2 dimensional data as wrapped one-dimensional data. This does not work always.

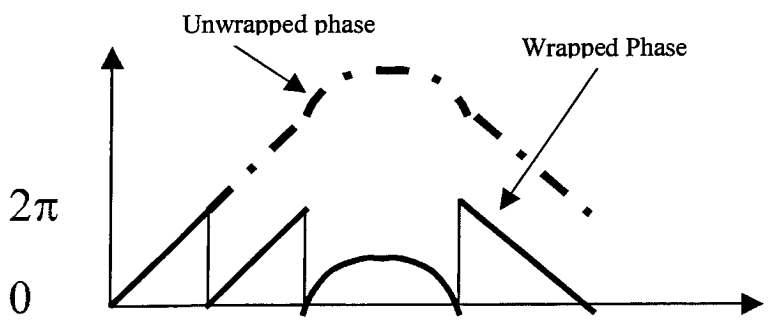

Figure 3.4.1: A representation of Phase wrapping.

An improved version was given Takeda [27]. Here each row is independently unwrapped. The rows now have an undetermined phase relation to each other. This is removed by scanning through the central column of each row sequentially. .

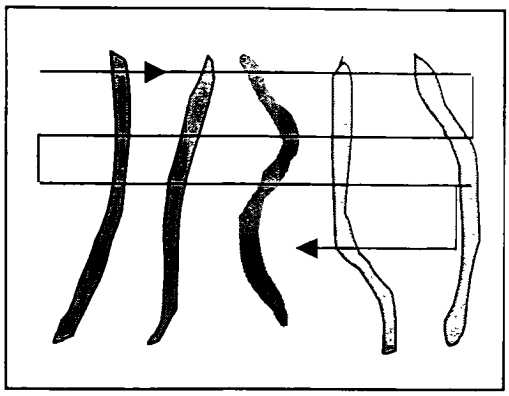

Line by line sequential unwrapping

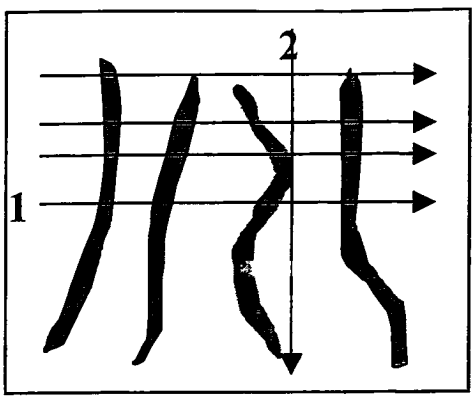

After Scan 1

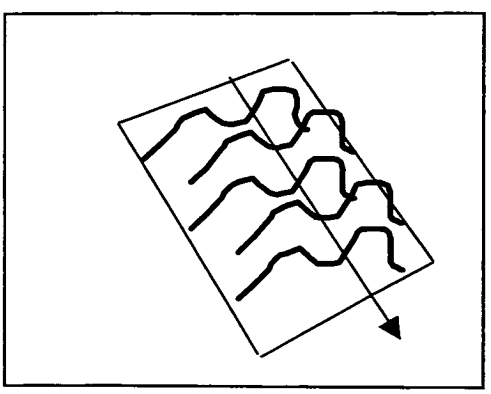

After Scan 2

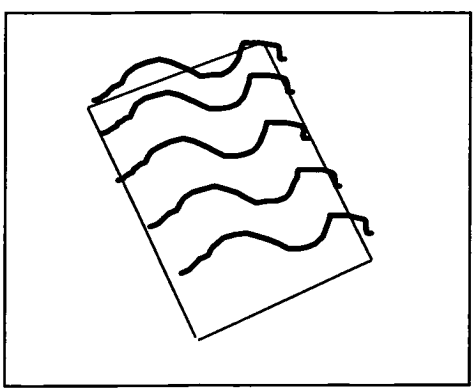

Takeda's method

Figure 3.4.2: Schematic of unwrapping by line-by-line method and Takeda's method.

4 Experimental set-up

A prototype experiment was done on an optic bench using a 436 nm Carl Zeiss optic. The set-up used was similar to that shown in figure 3.1.2. The source used was a He-Cd laser lasing at 442 nm. The object side pinhole was 10 microns. The grating used had a pitch of 80 microns and was kept a distance of 'z' away from the object pinhole, towards the optic. The grating was fabricated on commercially available, chrome plated glass masks using e-beam patterning. The image side mask was also fabricated using e-beam patterning. Initially the mask was made on commercially available, chrome plated masks, but these did not have enough attenuation. So glass plates were coated with 2000 angstroms of chrome and then used. The image side mask had a set of pinhole written with the small pinhole sizes ranging from 1 to 5 microns, for 2 different separations, 27.5 and 50 microns, corresponding to 'z' values of 50 and 90 mm. The pinhole pair with 1-micron size did not clear in the mask; possibly due to the inability of wet etch to clear the thicker chrome. From the data in the Table 4.1 the distance between the front lens surface and object plane is 440.5 mm and the distance between last lens surface and image plane is 29.4 mm.

For recording the interferogram an LBA 100 laser beam analyzer set-up was used. The LBA 100 uses a pulnix CCD camera (120 by 120 pixels). The data was transferred from the LBA 100 to a PC using an RS232 interface. The interferogram files were converted to TIF format from LBA format before being analyzed using an MATLAB

program written in-house for the purpose [Source code is in Appendix C]. A set of five typical interferograms is shown in the Figure 5.1.

S-Planar 1.6750

Cat. No.	10 77 82
Reduction ratio	1:10
Wavelength range	436+-5 nm
Object to Image distance	602+- 4mm
Image field diameter	14.5 mm
Square image format	10.5 by 10.5 mm
Flange focal distance	24.5 +- .3 mm
Free working distance	Min 10 mm
Length of barrel	160.5 mm
Max. diameter	85.5 mm
Screw thread	M 76 by 1
Entrance pupil Location behind the object Diameter	 486 mm 27.2 mm
Exit pupil Location behind the image Diameter	 512 mm 287 mm
Effective focal length	49.1 mm
Distance of Principal points	+ 8 mm
Numerical aperture	0.28
Diffraction limit of resolution	1285 line pair per/mm
Rayleigh depth in image space	+- 2.8 microns

Data on image performance

1. Full field

Distortion max. +- 0.3 microns

Optical transfer factor for incoherent/partially coherent illumination (σ=0.5)

Spatial frequency (lp per/mm)	Line width (um)	Optical Transfer function (%)
250	2	59/92
500	1	37/62
700	0.7	25/27

2. Restricted field diameter 10 mm

Distortion max. 0.2 microns

Optical Transfer factor for incoherent/partially coherent illumination (σ =0.5)

Spatial frequency (lp per/mm)	Line width (um)	Optical Transfer function (%)
250	2	69/96
500	1	46/67
700	0.7	30/30

Table 4.1: 436-nm Carl Zeiss lens data.

5 Results and Analysis

The experiment was performed on a Carl Zeiss g line lens. The procedure is explained in section 4.1. The experimental interferograms obtained for 0^0 orientation is shown in figure 5.1. The Wavefront aberration of the lens was calculated using the algorithms described. Park's method was used to remove the unsymmetrical aberrations due to the reference beam. An averaging of 50 counts was done while taking each interferogram to remove or reduce random errors. I used 2 fitting algorithms. These are shown in appendix C. Each algorithm was used to fit a synthetic wavefront for which all the Zernike coefficients were set to 0.1 waves. The difference or error wavefronts for each algorithm was calculated. The RMS for error wavefront after fitting, using algorithm 1 was 0.00754 waves, using algorithm 2 was 0.000247 waves. The values look small but are important as will be seen.

A set of six interferograms each having a phase difference of $\pi/2$ w.r.t the other was taken for all the 4 orientations. We can calculate the wavefront phase using 5-bucket algorithm. We should get comparable values when phase is calculated with the first 5 or the last 5 interferograms that is either using I_1, I_2, I_3, I_4, and I_5, or using I_2, I_3, I_4, I_5, and I_6. This should represent repeatability. The following plot Figure 5.2 shows the wavefront coefficients calculated using algorithm 1 and 2 for 90^0 orientation of the optic, by using the first 5 and last of the interferograms.

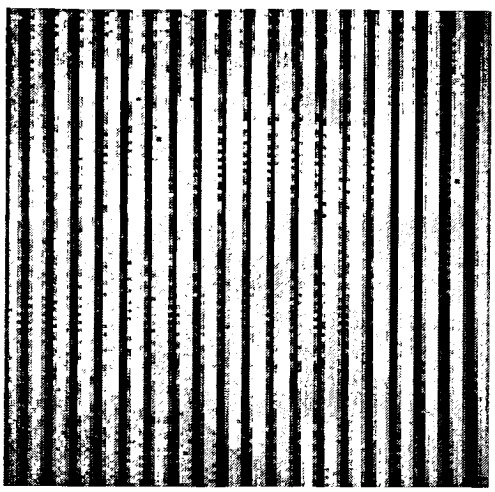

Interferogram 1

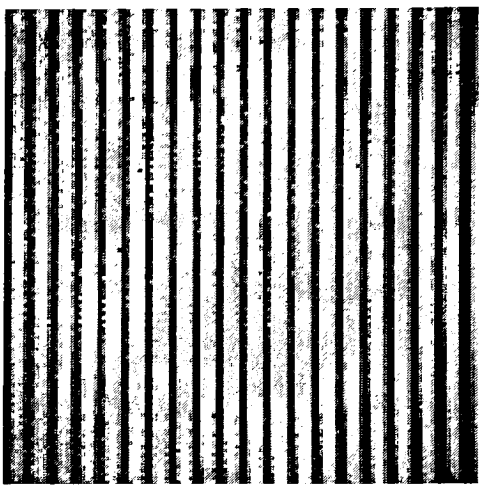

Interferogram 2

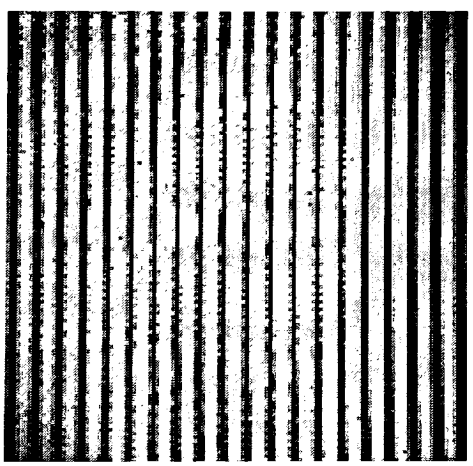

Interferogram 3

Figure 5.1: Shows a set interferograms shifted w.r.t each other by $\pi/2$. These interferograms were imaged on a 120 by 120 Pulnix CCD camera.

Interferogram 4

Interferogram 5

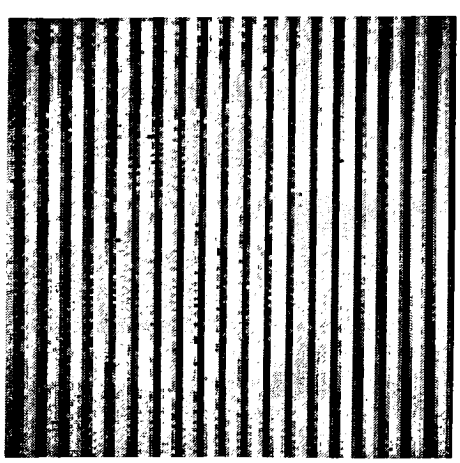

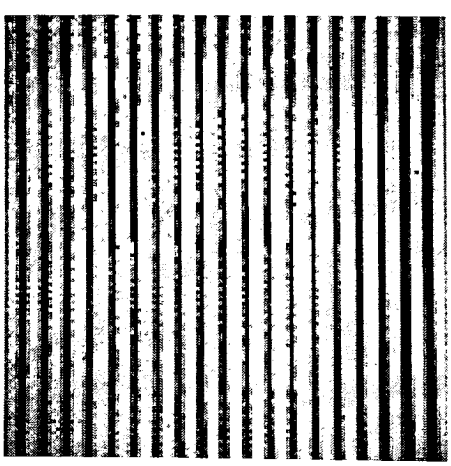

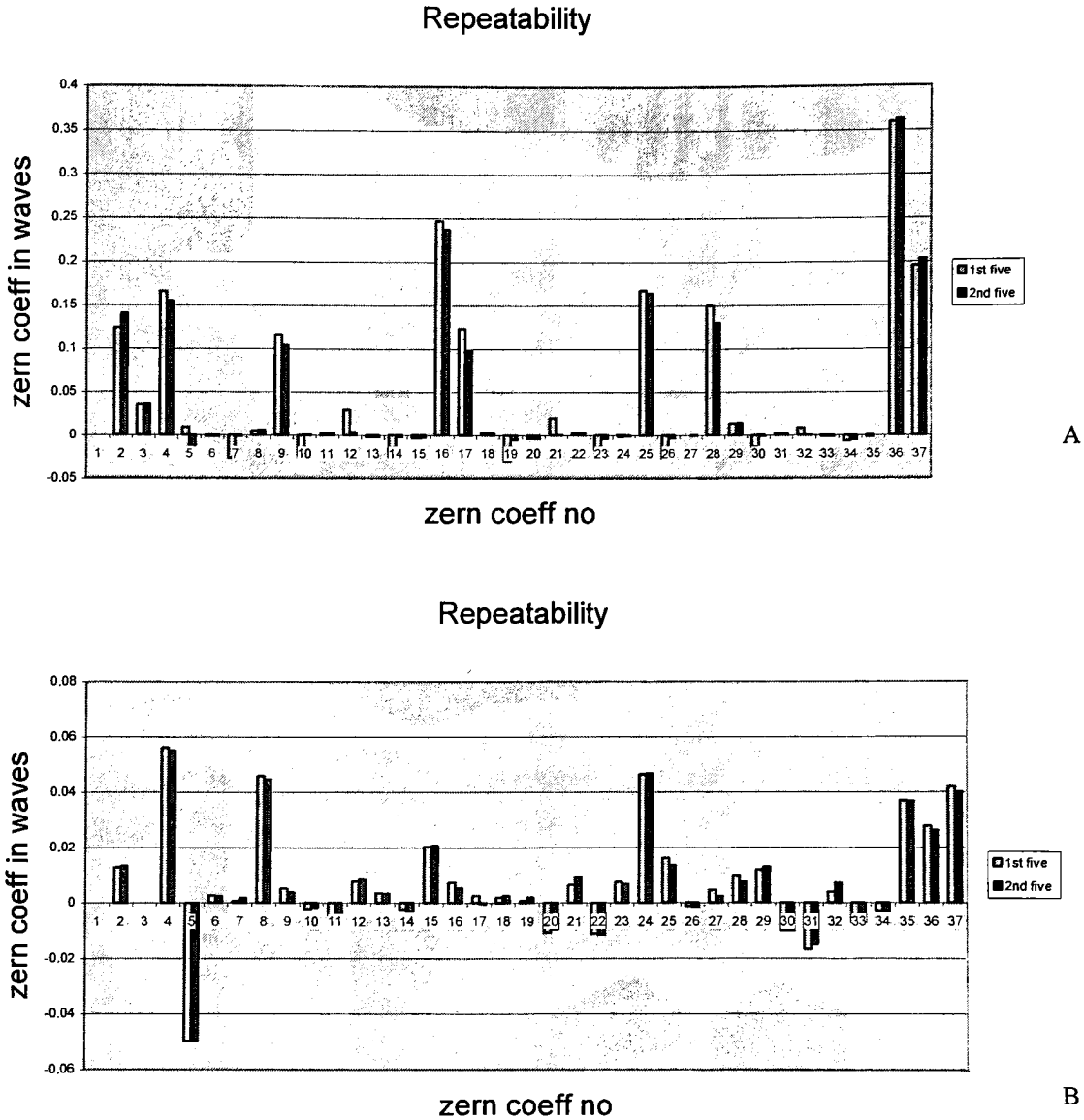

Figure 5.2: A shows the wavefront Zernike coefficients calculated using algorithm 1. B shows wavefront Zernike coefficients calculated using algorithm 2. For algorithm 1 the RMS of error wavefront is .0056 waves, and for algorithm 2 it is .0009 waves

The above plots indicate that repeatability is good and is independent of algorithm. The RMS values for the wavefronts match to within 0.0056 waves for algorithm 1 and within 0.0009 waves for algorithm 2. Algorithm 1 has more error in the estimating the following coefficients 9,10,15,16,17,28,36,37 and this is what leads to the larger values for these coefficients in the calculated wavefront. The comparison of the two algorithms is shown in Figure 5.3.

Tilt: The experimentally observed tilt in the interferogram, in line pairs per mm (lp/mm) is: observed tilt is 9.8666 waves or 19.73 lp/mm over 8.5 mm of CCD, that is 2.32 lp/mm. The calculated value from geometry using young's double slit equation: tilt in lp/mm is given by s/(λ*Z). Where 's' is the distance between the pinhole and window (27.5 microns), 'λ' is the wavelength (442 nm), and 'Z' is the distance between the pinhole mask and CCD plane (2.75 cm). Putting in the values, the tilt is found to be 2.26 lp/mm.

The values got from using algorithm 2 were used to calculate the wavefront coefficients for each of the 4 orientation of the optic. Park's method (Appendix B) was used to calculate the wavefront with reference errors removed. Figure 5.4 shows the aberration coefficients of the wavefront after applying Park's method. Strehl's Ratio calculated for the above wavefront is 0.91.

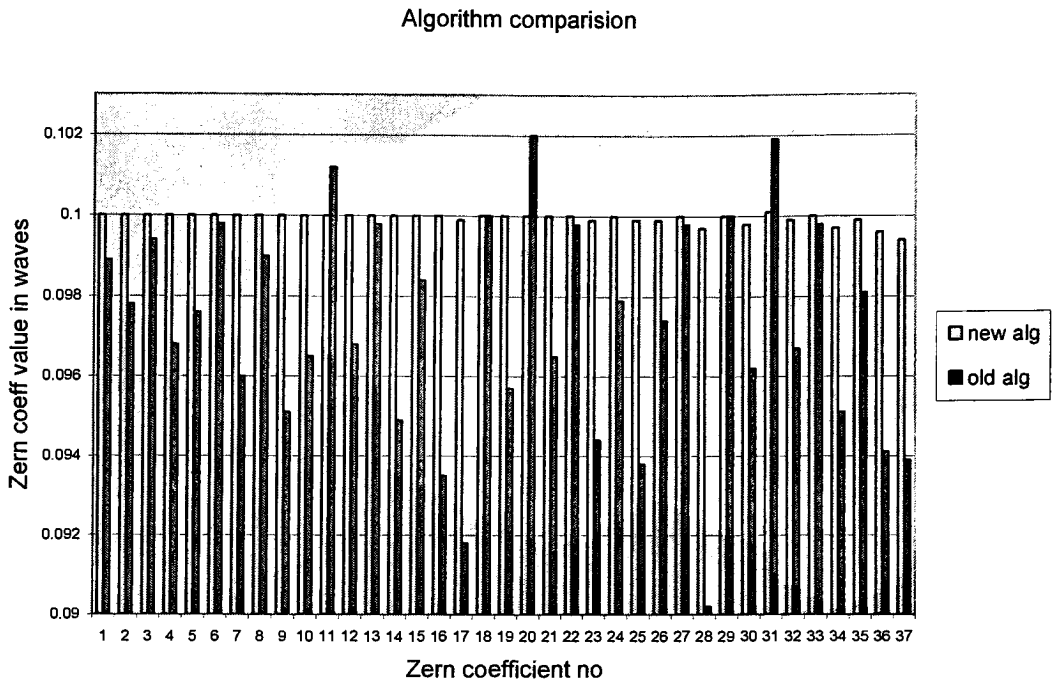

Figure 5.3: This shows the comparison of two algorithms used to fit the wavefront and estimate Zernike coefficients. Here fit is done to a synthetic wavefront with each coefficient having a value of 0.1. The maximum error for algorithm 1 occurs in the spherical terms.

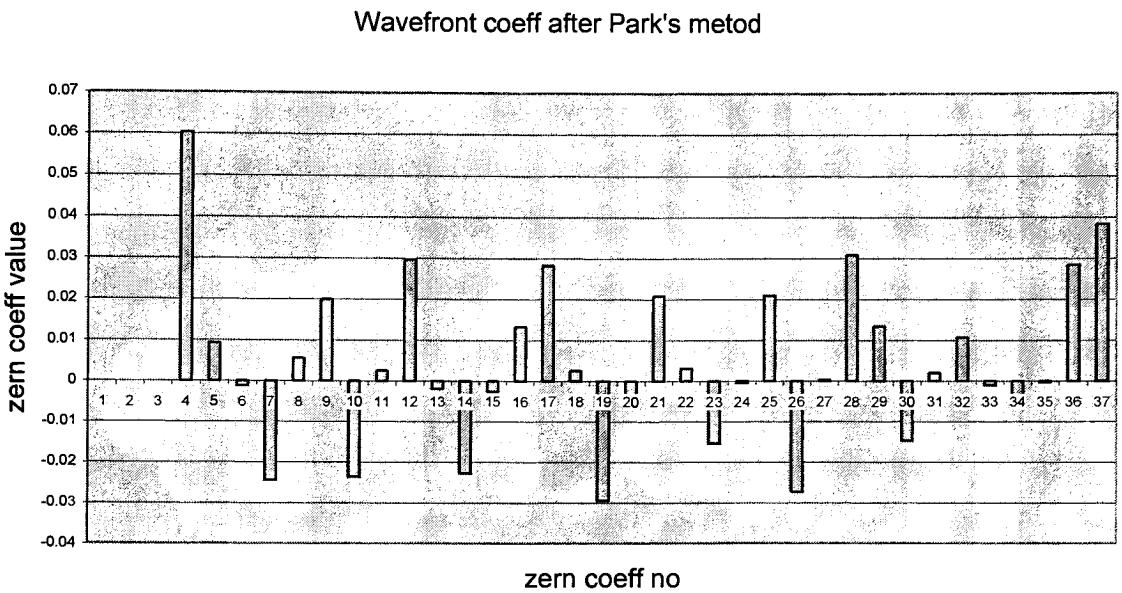

Figure 5.4: This shows the Zernike coefficients after applying Park's method. Algorithm 2 was used to do fitting.

MTF

The MTF of an optical system with known aberrations can be calculated using an equation from chapter 4 of 'The Art and Science of Optical Design', by R.R. Shannon [32].

The equations are:

$$
\begin{aligned}
DTF(\Omega) &= \frac{2}{\pi}[\arccos(\Omega) - \Omega\sqrt{1-\Omega^2}] \\
where \Omega &= \frac{\nu}{\nu_0} \\
ATF(\Omega) &= \left[1 - \left(\frac{W_{RMS}}{.18}\right)^2 \left(1 - 4(\Omega - 0.5)^2\right)\right] \\
MTF(\Omega) &= DTF(\Omega) ATF(\Omega)
\end{aligned}
\tag{5.1}
$$

In the above equations DTF is the aberration free MTF of lens, ATF is the aberration transfer lens depending on the Wavefront aberrations of the lens (W_{RMS}). Figure 5.5 shows the calculated MTF using the calculated W_{RMS} value of .0505 waves, and the MTF data given in the data sheet for the lens.

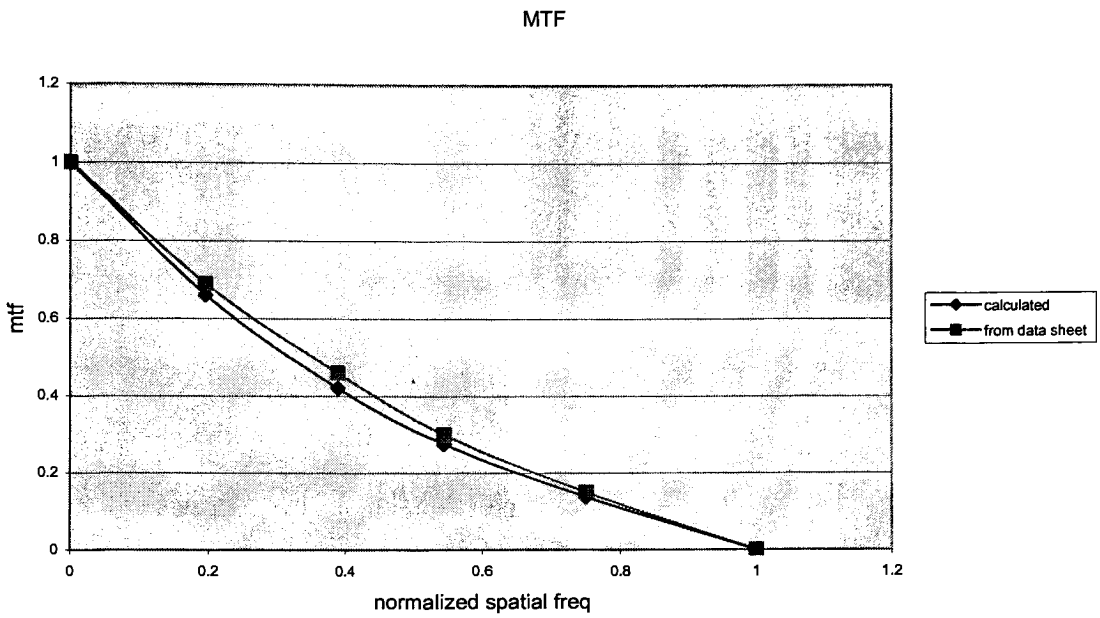

Figure 5.5: The above shows MTF plots of 436-nm optic from the datasheet and from calculation using the measured Strehl ratio, for comparison purposes.

Total error in the measurement:

1) Error due to grating glass plate: RMS of error wavefront is $7.92*10^{-5}$ waves
2) Error due to measurement (could include error due to grating motion, but I have considered that separately): RMS of error wavefront is 0.0009 waves.
3) Error due to motion of grating assuming I move to within 1 micron: RMS of error wavefront is 0.001587 waves.
4) Error due to detector tilt (assuming detector tilt is within 2 degrees to a plane normal to optic axis): RMS of error wavefront is 0.000188 waves

Assuming these errors to be independent the total error calculated for the measured wavefront is 0.0024119 waves for a measured wavefront RMS of 0.0505 waves.

6 Conclusions and Recommendations

The results obtained for the Zeiss lens show that PSPDI can be used for testing of stepper lenses. The measured values of aberrations and Strehl's ratio are in the expected order of magnitude. The analysis end has been verified and works fine. The things learned are that one of the most crucial components is the sub-resolution pinhole. The smaller the pinhole is, the better the accuracy of the measured aberrations. But one has to keep also in mind that the smaller pinhole will reduce the contrast in the interferogram. The set-up can be calibrated by using a 2-sub-resolution pinhole mask and calculating the coma got from interferogram analysis, and comparing the result with expected coma for the set-up (refer section 3.2.4). The grating motion needs to be calibrated and micrometer stages with accuracy of 0.1 micron need to be used as mentioned in section 3.2.2. As mentioned in section 3.2.3 for future measurements one needs to take averages of measurements by moving the pinhole mask by a fraction of the optic PSF and also taking averages over a number of pinhole pairs. One can get a better estimate of the total error by doing the following:

a) Measurement error: Take 10 interferograms shifted w.r.t each other by a phase of $\pi/2$, this allows for calculation of wavefront phase 5 times. This implies I can generate 10 difference wavefronts. Let the standard deviation of the RMS of these difference wavefronts be σ_1.

b) Make another set of measurements with the position of micrometer screw moving the grating, moved by .2 micron from ideal position for each of the five successive positions. Calculate the wavefront phase for each case; calculate the difference wavefront w.r.t ideal case. Let σ_2 be the standard deviation of the RMS of these difference wavefronts.

c) Let σ_3 represent the RMS of the error wavefront due to glass plate(grating)

d) Let σ_4 represent the RMS of the error wavefront due to detector tilt (assuming detector plane is normal to optic axis within 1 degree).

The total error in the RMS of measured wavefront then is:

$$\sigma = \left(\frac{\sigma_1^2}{10} + \frac{\sigma_2^2}{5} + \sigma_3^2 + \sigma_4^2\right)^{.5} \tag{6.1}$$

One can do a similar analysis for each Zernike coefficient individually.

Appendix A

Zernike fitting

We now discuss the vector formulation for Zernike polynomial surface fitting and extraction of Zernike coefficients. A wavefront can be represented as a linear combination of Zernike polynomials.

$$W(x,y) = \sum_j a_j Z_j(x,y) \tag{1}$$

In discrete form:

$$W_r(x_r,y_r) = \sum_{j=1}^{m} a_j Z_j(x_r,y_r) \tag{2}$$

Where W_r (x_r, yr) is the value of wavefront at point (x_r, y_r) and Z_j's are Zernike polynomials and a_j's are the coefficients. Let there be n points ($n>m$). Usually m = 37. Writing the above in matrix form

$$\begin{bmatrix} W_1(x_1,y_1) \\ W_2(x_2,y_2) \\ \\ \\ W_n(x_n,y_n) \end{bmatrix} = \begin{bmatrix} Z_1(x_1,y_1), \text{----------} Z_m(x_1,y_1) \\ Z_1(x_2,y_2), \text{----------} Z_m(x_2,y_2) \\ \\ \\ Z_1(x_n,y_n), \text{----------} Z_m(x_n,y_n) \end{bmatrix} * \begin{bmatrix} a_1 \\ \\ \\ a_m \end{bmatrix} \tag{3}$$

Writing

$$\begin{bmatrix} W_1 \\ W_2 \\ \\ \\ W_n \end{bmatrix} = \underline{W}, \begin{bmatrix} Z_j(x_1, y_1) \\ Z_j(x_2, y_2) \\ \\ \\ Z_j(x_n, y_n) \end{bmatrix} = \underline{Z_j}, \begin{bmatrix} a_1 \\ a_2 \\ \\ \\ a_n \end{bmatrix} = \underline{a} \tag{4}$$

using (3), equation (2) can be written as:

$$\underline{W}=[\underline{Z_1}, \underline{Z2}, \text{----------}, \underline{Zm}]*\underline{a} \tag{5}$$

Let the measured value of actual wavefront $\underline{W}$ be given by $\underline{W1}$. Then sum of squares is given by:

$$S = [\underline{W1} - [\underline{Z_1}, \text{----------}, \underline{Zm}]*\underline{a}]^2 \tag{6}$$

that is:

$$S = \sum_{r=1}^{n} (W1_r - \sum_{j=1}^{m} a_j Z_j(x_r, y_r)\}^2 \tag{7}$$

Now minimizing S w.r.t a_j we get:

$$\sum_{r=1}^{n} W1_r Z_k(x_r, y_r) = \sum_{r=1}^{n} \sum_{j=1}^{m} a_j Z_j(x_r, y_r) Z_k(x_r, y_r) \tag{8}$$

In matrix form we have:

$$\begin{bmatrix} W1Z_1 \\ \\ \\ W1Z_m \end{bmatrix} = \begin{bmatrix} Z_1Z_1, \text{------}, Z_1Z_m \\ Z_2Z_1, \text{------}, Z_2Z_m \\ \\ \\ Z_mZ_1, \text{------}, Z_mZ_m \end{bmatrix} * \begin{bmatrix} a_1 \\ \\ \\ a_m \end{bmatrix} \tag{9}$$

Choosing Z_j's to be orthonormal one has:

$$\begin{bmatrix} W1Z_1 \\ \\ \\ W1Z_m \end{bmatrix} = \begin{bmatrix} Z_1Z_1, 0, \text{----------}, 0 \\ 0, Z_2Z_2, \text{----------}, 0 \\ \\ \\ 0, 0, \text{----------}, Z_mZ_m \end{bmatrix} * \begin{bmatrix} a_1 \\ \\ \\ a_m \end{bmatrix} \tag{10}$$

The coefficients can then be written as:

$$\underline{a} = \begin{bmatrix} \dfrac{W1Z_1}{|Z_1|^2} \\ \\ \\ \dfrac{W1Z_m}{|Z_m|^2} \end{bmatrix} \tag{11}$$

Because we are using discrete set of data we need to orthonormalize over the given set of discrete data using Gram-Schmidt orthogonalization. If Z_j's are the original Zernike polynomials, then letting the polynomials, which are orthogonal over the data set, to be $Z1_j$'s we have using Gram-Schmidt orthogonalization.

$$Z1_1 = Z_1 \tag{12}$$

$$Z1_s = Z_j - \sum_{s=1}^{j-1} D_{js} Z1_s \tag{13}$$

$$D_{js} = \frac{Z_j * Z1_s}{Z1_s * Z1_s} \tag{14}$$

Then writing measured wavefront in terms of the new orthogonal polynomials:

$$\underline{W1} = [Z1_1 \text{ ---} Z1_m] * \underline{b} \tag{15}$$

$$\text{Or } \underline{b} = \begin{bmatrix} W1Z1_1 \\ \\ \\ W1Z1_m \end{bmatrix} \tag{16}$$

where $\underline{b}$ is the set of new coefficients.

Orthogonalization equation in matrix form can be written as:

$$\begin{bmatrix} Z1_1^T \\ \\ \\ Z1_m^T \end{bmatrix} = \begin{bmatrix} Z_1^T \\ \\ \\ Z_m^T \end{bmatrix} - \begin{bmatrix} 0000000---00000000 \\ D_{21}000000---0000000 \\ D_{31}D_{32}0-----000000 \\ \\ \\ D_{m1}D_{m2}-------D_{mm-1}0 \end{bmatrix} \begin{bmatrix} Z1_1^T \\ \\ \\ Z1_m^T \end{bmatrix} \tag{17}$$

or

$$\begin{bmatrix} Z1_1^T \\ \\ \\ Z1_m^T \end{bmatrix} = [I + D]^{-1} \begin{bmatrix} Z_1^T \\ \\ \\ Z_m^T \end{bmatrix} \tag{18}$$

Where I is an m by m Identity matrix and D is the matrix of the D_{js} coefficients.

Equating (4) and (14) we get:

$$[Z_1,-------,Z_m]\underline{a} = [Z1_1,-----,Z1_m]\underline{b} \tag{19}$$

Rewriting (17) as:

$$[Z_1,-----,Z_m]^T = (I+D)^{-1}[Z1_1,-----,Z1_m]^T \tag{20}$$

Taking transpose of above equation and using (18) one gets:

$$\underline{a} = ((I+D)^{-1})^T \underline{b} \tag{21}$$

The results of the algorithm fit are shown in the following graphs. A wavefront with known coefficient values for all 37 Zenike polynomials (data from a 193-nm lens from Tropel) was generated and the above method used to fit Zernike coefficients to the wavefront. This was done for different array sizes. A good way to check the fit is to compute the wavefront rms of the difference wavefront. This is nothing but the square root of the sum of squares of the renormalized Zernike coefficients except the first one.

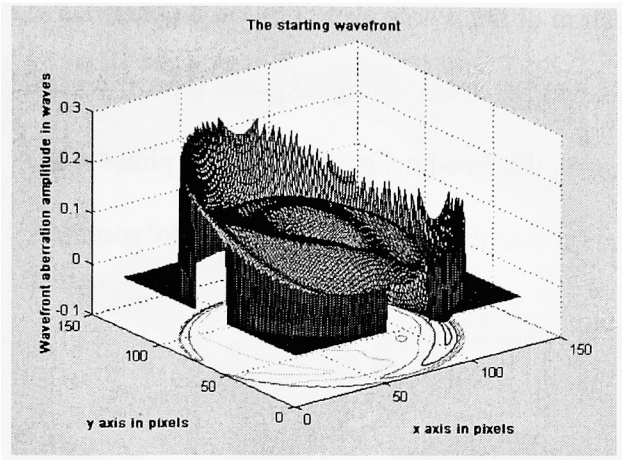

A

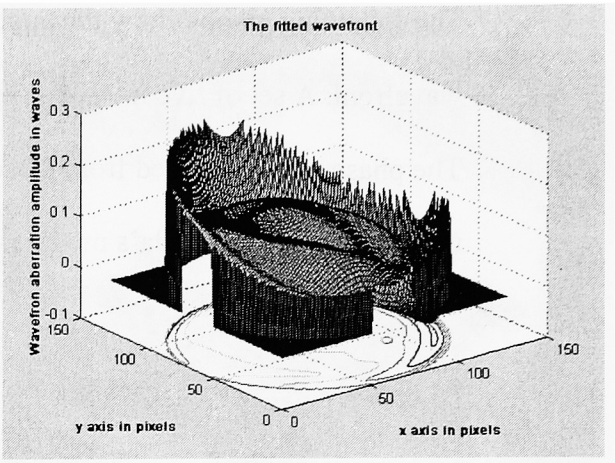

B

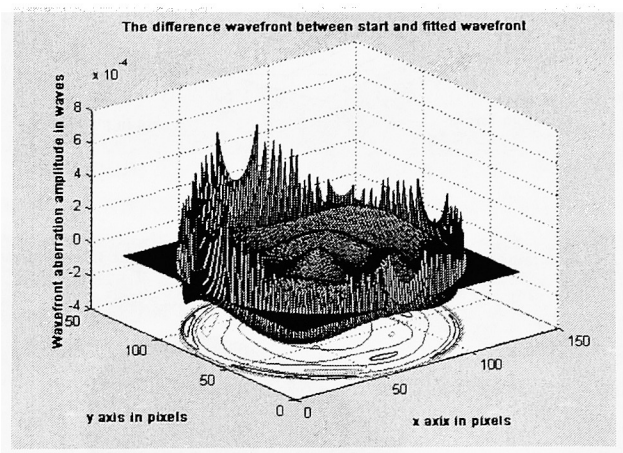

C

Figure A1: A is the wavefront generated using known coefficients, B is the fitted wavefront, and C is the difference wavefront. The RMS values are 0.058559, 0.058558, and 0.000001 waves respectively for A, B, and C. Algorithm 2 was used for fitting.

The following graphs show the application of the whole algorithm on a generated wavefront. A set of five interferograms was generated using a known typical wavefront. The phase was calculated from these using the five-bucket method. The phase was unwrapped using Takeda's method and the wavefront fit to 37 Zernike polynomials.

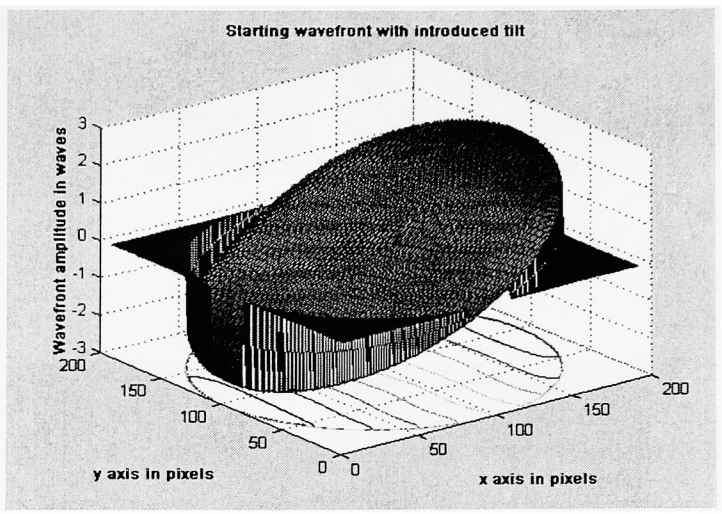

A

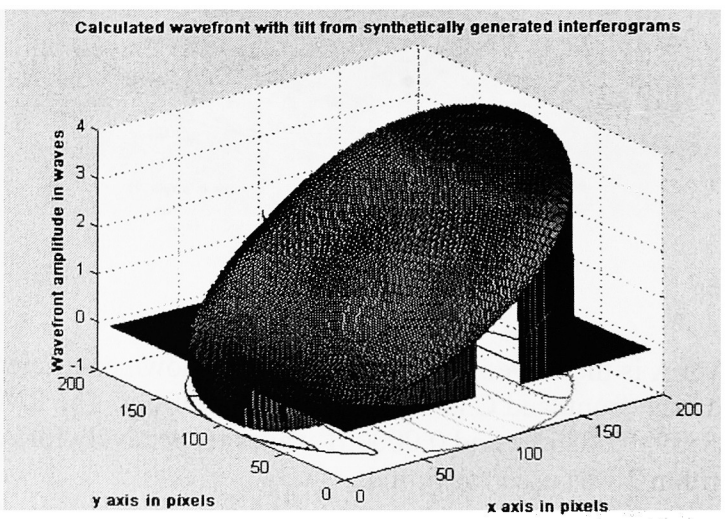

B

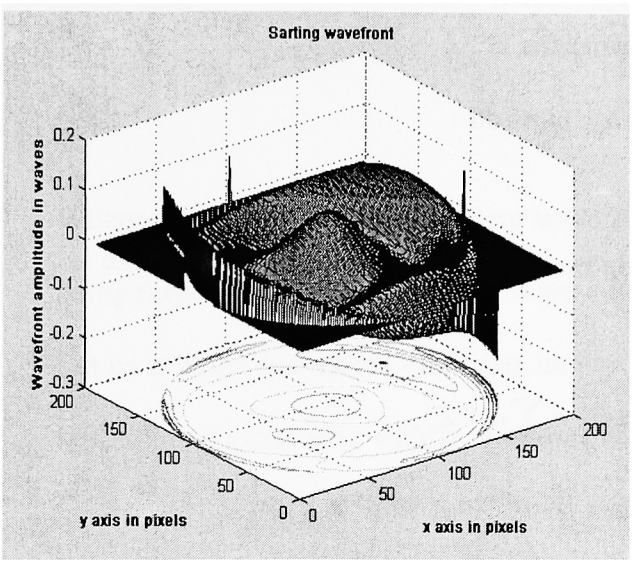

C

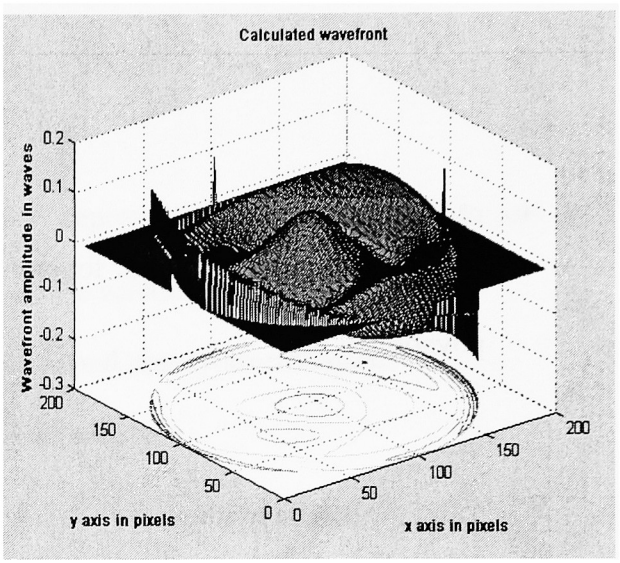

D

Figure A2: This figure shows the performnce of the whole algorithm. A is the generated wavefront. B is the wavefront obtained from A after generating 5 interferograms, getting phase from them, unwrapping the phase and then doing a zernke fit. C is the wavefront in A without the tilt term. D is the wavefront in B without the tilt and piston.

Appendix B

Park's method

Error wavefront error for any optic can be represented in terms of Zernike poynomials as:

$$W(\rho,\theta) = \sum_i a_i * Z_i \tag{1}$$

This can also be written as:

$$\mathrm{W}\ (\rho,\theta) = \sum_{l,k} R_l^k(\rho) * (a_l^k * Cos(k\vartheta) + a_l^{-k} * Sin(k\vartheta)) \tag{2}$$

Where $R_l^k(\rho)$ are the radial terms of the polynomial, the angular terms represent azimuthal part of the polynomial. The wavefront error data is usually calculated from a set of interferograms.

When a part of a lens assembly or the assembly itself is rotated by an angle ϕ, it affects only the azimuthal coefficients in the error wavefront error. Knowing the effect of rotation on azimuthal terms one can then calculate the coefficients of the rotated part from the wavfront data for part with and without rotation. It should be noted that we cannot calculate the azimuthal coefficients with k=0, as these represent symmetric wavefront error terms and do not change on rotation.

In any interference set up the wavefront error measured is the sum of wavefront errors due to part and reference,

$$W(\rho,\theta) = P(\rho,\theta) + R(\rho,\theta) \tag{3}$$

Where 'W' represents the total error wavefront, 'P' represents error wavefront due to part being measured; 'R' represents error wavefront due to reference.

Let us split the Wavefront error data into symmetric and non-symmetric parts, representing symmetric with 's' and unsymmetrical with 'u':

$$W_S(\rho,\theta) + W_U(\rho,\theta) = P_S(\rho,\theta) + R_S(\rho,\theta) + P_U(\rho,\theta) + R_U(\rho,\theta) \tag{4}$$

$$W_S(\rho,\theta) + W_U(\rho,\theta) =$$

$$\sum_{l,k=0} R_l^k(\rho) * ((a_l^k + b_l^k) * Cos(k\vartheta) + (a_l^{-k} + b_l^{-k}) * Sin(k\vartheta)) +$$
$$\sum_{l,k|=0} R_l^k(\rho) * ((a_l^k + b_l^k) * Cos(k\vartheta) + (a_l^{-k} + b_l^{-k}) * Sin(k\vartheta)) \tag{5}$$

Where coefficients 'a' and 'b' represent the coefficients of part and reference respectively, also the k=0 terms represent symmetric error terms and k|=0 represents the nonsymmetrical terms.

On rotating the part by 'ϕ' the wavefront error changes as:

$$W_S(\rho,\theta) + W_U(\rho,\theta+\phi) = P_S(\rho,\theta) + R_S(\rho,\theta) + P_U(\rho,\theta+\phi) + R_U(\rho,\theta) \tag{6}$$

$$W_S(\rho,\theta)+W_U(\rho,\theta+\phi)=$$

$$\begin{aligned}&\sum_{l,k=0} R_l^k(\rho)*((a_l^k+b_l^k)*Cos(k\vartheta)+(a_l^{-k}+b_l^{-k})*Sin(k\vartheta))+\\&\sum_{l,k|=0} R_l^k(\rho)*((a1_l^k+b_l^k)*Cos(k\vartheta)+(a1_l^{-k}+b_l^{-k})*Sin(k\vartheta)\end{aligned} \tag{7}$$

where:

$$a1_l^{+-k}=a_l^{+-k}*Cos(k\phi)+-a_l^{-+k}*Sin(k\phi) \tag{8}$$

If we now rotates the above wavefront synthetically using software by'-ϕ', we have:

$$W_S(\rho,\theta)+W_U(\rho,\theta)=P_S(\rho,\theta)+R_S(\rho,\theta)+P_U(\rho,\theta)+R_U(\rho,\theta) \tag{9}$$

$$\text{Ws }(\rho,\theta)+\text{Wu }(\rho,\theta)=$$

$$\begin{aligned}&\sum_{l,k=0} R_l^k(\rho)*((a_l^k+b_l^k)*Cos(k\vartheta)+(a_l^{-k}+b_l^{-k})*Sin(k\vartheta))+\\&\sum_{l,k|=0} R_l^k(\rho)*((a2_l^k+b1_l^k)*Cos(k\vartheta)+(a2_l^{-k}+b1_l^{-k})*Sin(k\vartheta))\end{aligned} \tag{10}$$

where:

$$a2_l^{+-k}=a1_l^{+-k}*Cos(-k\phi)+-a1_l^{-+k}*Sin(-k\phi) \tag{11}$$

$$b1_l^{+-k}=b_l^{+-k}*Cos(-k\phi)+-b_l^{-+k}*Sin(-k\phi) \tag{12}$$

that is:

$$\begin{aligned}&a2_l^{+-k}=(a_l^{+-k}*Cos(k\phi)+-a_l^{-+}*Sin(k\phi))*Cos(-k\phi)\\&+-(a_l^{-+k}*Cos(k\phi)--+a_l^{+-k}*Sin(k\phi))*Sin(-k\phi)\end{aligned} \tag{13}$$

On solving one gets:

$$a2_l^{+-1} = a_l^{+-1} \tag{14}$$

If we take wavefront data with the test object at 'n' equally spaced azimuthal locations with respect to the interferometer, rotate the data back synthetically and take the average all the errors of nonzero orders that not harmonics of 'n' are removed. After averaging one is left with:

$$W(\rho, \vartheta) = Ps(\rho, \vartheta) + Rs(\rho, \vartheta) + Pu(\rho, \vartheta) \tag{15}$$

Appendix C

Algorithm difference

Algorithm difference: The difference in the algorithm mentioned is basically the difference in the way the Gram-Schmidt Algorithm was implemented. The following page shows the 2 versions employed. Version 2 gives better results as shown in the results section of thesis.

Version 1:

```
ort=double(W);
orto=zeros(s,s,l);
        for i=1:l
           orto(:,:,i)=ort(:,:,i)/(trace(ort(:,:,i)'*ort(:,:,i)));
           for j=i+1:l
             d(i,j)=trace(orto(:,:,i)'*ort(:,:,j));
              ort(:,:,j)=ort(:,:,j)-d(i,j)*orto(:,:,i);
           end
       end
```

Version 2:

```
ortoo=zeros(s,s,l);
orto=zeros(s,s,l);
ort=zeros(s,s,l);
ort=double(ort);
for i=1:s
   for j=1:s
      ort(i,j,1) = W(i,j,1);
   end
end

              for i=2:l

           for  j=1:i-1

d(i,j)=trace(W(:,:,i)'*ort(:,:,j))/(trace(ort(:,:,j)'*ort(:,:,j)));
```

```
            orto(:,:,j)=d(i,j)*W(:,:,j);
              ortoo(:,:,i)=orto(:,:,j)+ortoo(:,:,i);
                end
    ort(:,:,i)=W(:,:,i)-ortoo(:,:,i);


        end;
```

The following is a copy of the whole matlab program which reads in the interferogram "tif" files, applies 5-bucket algorithm to calculate phase, use Takeda's method to unwrap the phase, apply Gram-Schmidt algorithm to do fitting and determine the Zernike coefficients.

```
% This program calculates phase by 5-bucket method
% unwraps phase using Takeda's method
% uses Gram-Schmidt algorithm to fit and determine
% Zernike coefficients of the calculated wavefront


% The five tiff files are read
L1=imread('2171','tif');
L2=imread('2172','tif');
L3=imread('2173','tif');
L4=imread('2174','tif');
L5=imread('2175','tif');
L1=double(L1);
L2=double(L2);
L3=double(L3);
L4=double(L4);
L5=double(L5);
s=size(L1,1);
tre=zeros(1,5);

% the following is a provision to remove spikes by
% using median filtering if need be

%phi=double(phi);
    %  for i=2:s-1
   %for j=2:s-1
    %  tre=[L1(i-1,j),L1(i,j-1),L1(i,j),L1(i,j+1),L1(i+1,j)];
     % L1(i,j)=median(tre);
```

```
   %end
%end
%for i=2:s-1
 %  for j=2:s-1
  %     tre=[L2(i-1,j),L2(i,j-1),L2(i,j),L2(i,j+1),L2(i+1,j)];
   %    L2(i,j)=median(tre);
   %end
%end
%for i=2:s-1
 %  for j=2:s-1
  %     tre=[L3(i-1,j),L3(i,j-1),L3(i,j),L3(i,j+1),L3(i+1,j)];
   %    L3(i,j)=median(tre);
   %end
%end
%for i=2:s-1
 %  for j=2:s-1
  %     tre=[L4(i-1,j),L4(i,j-1),L4(i,j),L4(i,j+1),L4(i+1,j)];
   %    L4(i,j)=median(tre);
    %end
    %end
%for i=2:s-1
 %  for j=2:s-1
  %     tre=[L5(i-1,j),L5(i,j-1),L5(i,j),L5(i,j+1),L5(i+1,j)];
   %    L5(i,j)=median(tre);
   %end
%end



% The 5-bucket method
for p=1:s
   for q=1:s
      L0(p,q)=(L2(p,q)-L4(p,q))/2;
      L01(p,q)=(2*L3(p,q)-L5(p,q)-L1(p,q))/4;

                                    end;
                                end;

                            phi=atan2(L0,L01);


We=phi;
s=size(We,1);
We1=zeros(s,s);
We1=double(We1);
s1=s/2;
a1=0;
b1=s1;
```

```
% median filtering to remove spikes
for i=2:s-1
  for j=2:s-1

              tre=[We(i-1,j),We(i+1,j),We(i,j),We(i,j-1),We(i,j+1)];
             We1(i,j)=median(tre);

          end
end


% Definition of Zernike polynomials, creating polynomials
% upto order 9
s=120;
s1=s/2;
a1=0;
b1=s1;


for x=1:s
    for y=1:s
       if (((x-s1)/s1)^2+((y-s1)/s1)^2)>=a1^2/(s1)^2 & (((x-
s1)/s1)^2+((y-s1)/s1)^2)<=b1^2/(s1)^2
          Wr(x,y,1)=mod((((x-s1)/s1)^2+((y-s1)/s1)^2)^.5,1);
          Wa1(x,y,1)=(y-s1)/s1;
          Wa2(x,y,1)=(x-s1)/s1;
       else
          Wr(x,y,1)=0;
          Wa1(x,y,1)=0;

          Wa2(x,y,1)=0;
      end
    end
 end
 Wa1=double(Wa1);
 Wa2=double(Wa2);
 Wa=atan2(Wa1,Wa2);
 Wa=double(Wa);

for x=1:s
   for y=1:s

      if (((x-s1)/s1)^2+((y-s1)/s1)^2)>=a1^2/(s1)^2 & (((x-
s1)/s1)^2+((y-s1)/s1)^2)<=b1^2/(s1)^2



          W(x,y,1)=1;
          W(x,y,2)=Wr(x,y,1)*cos(Wa(x,y,1));
          W(x,y,3)=Wr(x,y,1)*sin(Wa(x,y,1));
```

```
            W(x,y,4)=2*Wr(x,y,1)^2-1;
            W(x,y,5)=Wr(x,y,1)^2*cos(2*Wa(x,y,1));
            W(x,y,6)=Wr(x,y,1)^2*sin(2*Wa(x,y,1));
            W(x,y,7)=(3*Wr(x,y,1)^3-2*Wr(x,y,1))*cos(Wa(x,y,1));
            W(x,y,8)=(3*Wr(x,y,1)^3-2*Wr(x,y,1))*sin(Wa(x,y,1));
            W(x,y,9)=6*Wr(x,y,1)^4-6*Wr(x,y,1)^2+1;
            W(x,y,10)=Wr(x,y,1)^3*cos(3*Wa(x,y,1));
            W(x,y,11)=Wr(x,y,1)^3*sin(3*Wa(x,y,1));
            W(x,y,12)=(4*Wr(x,y,1)^4-3*Wr(x,y,1)^2)*cos(2*Wa(x,y,1));
            W(x,y,13)=(4*Wr(x,y,1)^4-3*Wr(x,y,1)^2)*sin(2*Wa(x,y,1));
            W(x,y,14)=(10*Wr(x,y,1)^5-
12*Wr(x,y,1)^3+3*Wr(x,y,1))*cos(Wa(x,y,1));
            W(x,y,15)=(10*Wr(x,y,1)^5-
12*Wr(x,y,1)^3+3*Wr(x,y,1))*sin(Wa(x,y,1));
            W(x,y,16)=20*Wr(x,y,1)^6-30*Wr(x,y,1)^4+12*Wr(x,y,1)^2-1;
            W(x,y,17)=Wr(x,y,1)^4*cos(4*Wa(x,y,1));
            W(x,y,18)=Wr(x,y,1)^4*sin(4*Wa(x,y,1));
            W(x,y,19)=(5*Wr(x,y,1)^5-4*Wr(x,y,1)^3)*cos(3*Wa(x,y,1));
            W(x,y,20)=(5*Wr(x,y,1)^5-4*Wr(x,y,1)^3)*sin(3*Wa(x,y,1));
            W(x,y,21)=(15*Wr(x,y,1)^6-
20*Wr(x,y,1)^4+6*Wr(x,y,1)^2)*cos(2*Wa(x,y,1));
            W(x,y,22)=(15*Wr(x,y,1)^6-
20*Wr(x,y,1)^4+6*Wr(x,y,1)^2)*sin(2*Wa(x,y,1));
            W(x,y,23)=(35*Wr(x,y,1)^7-60*Wr(x,y,1)^5+30*Wr(x,y,1)^3-
4*Wr(x,y,1))*cos(Wa(x,y,1));
            W(x,y,24)=(35*Wr(x,y,1)^7-60*Wr(x,y,1)^5+30*Wr(x,y,1)^3-
4*Wr(x,y,1))*sin(Wa(x,y,1));
            W(x,y,25)=70*Wr(x,y,1)^8-140*Wr(x,y,1)^6+90*Wr(x,y,1)^4-
20*Wr(x,y,1)^2+1;
            W(x,y,26)=Wr(x,y,1)^5*cos(5*Wa(x,y,1));
            W(x,y,27)=Wr(x,y,1)^5*sin(5*Wa(x,y,1));
            W(x,y,28)=(6*Wr(x,y,1)^6-5*Wr(x,y,1)^4)*cos(4*Wa(x,y,1));
            W(x,y,29)=(6*Wr(x,y,1)^6-5*Wr(x,y,1)^4)*sin(4*Wa(x,y,1));
            W(x,y,30)=(21*Wr(x,y,1)^7-
30*Wr(x,y,1)^5+10*Wr(x,y,1)^3)*cos(3*Wa(x,y,1));
            W(x,y,31)=(21*Wr(x,y,1)^7-
30*Wr(x,y,1)^5+10*Wr(x,y,1)^3)*sin(3*Wa(x,y,1));
            W(x,y,32)=(56*Wr(x,y,1)^8-105*Wr(x,y,1)^6+60*Wr(x,y,1)^4-
10*Wr(x,y,1)^2)*cos(2*Wa(x,y,1));
            W(x,y,33)=(56*Wr(x,y,1)^8-105*Wr(x,y,1)^6+60*Wr(x,y,1)^4-
10*Wr(x,y,1)^2)*sin(2*Wa(x,y,1));
            W(x,y,34)=(126*Wr(x,y,1)^9-280*Wr(x,y,1)^7+210*Wr(x,y,1)^5-
60*Wr(x,y,1)^3+5*Wr(x,y,1))*cos(Wa(x,y,1));
            W(x,y,35)=(126*Wr(x,y,1)^9-280*Wr(x,y,1)^7+210*Wr(x,y,1)^5-
60*Wr(x,y,1)^3+5*Wr(x,y,1))*sin(Wa(x,y,1));
            W(x,y,36)=252*Wr(x,y,1)^10-630*Wr(x,y,1)^8+560*Wr(x,y,1)^6-
210*Wr(x,y,1)^4+30*Wr(x,y,1)^2-1;
            W(x,y,37)=924*Wr(x,y,1)^12-
2772*Wr(x,y,1)^10+3150*Wr(x,y,1)^8-1680*Wr(x,y,1)^6+420*Wr(x,y,1)^4-
42*Wr(x,y,1)^2+1;
```

```
else W(i,j,:)=0;
   end;

                    end;
 end;
W=double(W);
n=0;
s=120;
We2=zeros(s,s);

% Application of Takeda's method for phase unwrapping
for i=1:s
   n1=0;
   n2=0;

   for j=2:s
      if  (We1(i,j)-We1(i,j-1))>=pi


                    for k=j:s

            We1(i,k)=We1(i,k)-2*pi;
            end
                   elseif (We1(i,j)-We1(i,j-1))<=-pi
                       for k=j:s

            We1(i,k)=We1(i,k)+2*pi;

            end



      end
   end

end
We1(:,1)=.5*(We1(:,2)+We1(:,3));
phil0=zeros(s,s);
s1=s/2;
for i=2:s
   if We1(i,s/2)-We1(i-1,s/2)>=pi
            for k=1:s
         We1(i,k)=We1(i,k)-2*pi;
      end
   elseif We1(i,s/2)-We1(i-1,s/2)<=-pi
      for k=1:s
         We1(i,k)=We1(i,k)+2*pi;
      end
```

```
     end
  end
  Wel(1,:)=.5*(Wel(2,:)+Wel(3,:));

for i=1:s
       Wel(120,i)=Wel(120,i)+pi;


  end

% bounding the phase calculated to a unit circle
for i=1:120
   for j=1:120
      if ((i-s1)/s1)^2+((j-s1)/s1)^2<=1
         phi10(i,j)=Wel(i,j);
      else phi10(i,j)=0;
      end
   end
end
% median filtering if need be
    % for i=2:s-1
  % for j=2:s-1

         %     tre=[phi10(i-1,j),phi10(i+1,j),phi10(i,j),phi10(i,j-
1),phi10(i,j+1)];
         %    phi10(i,j)=median(tre);

        %   end
       % end




l=37;
d=zeros(1,l);
% the first version of Gram-Schmidt algorithm
%%
%ort=double(W);
%orto=zeros(s,s,l);
 %       for i=1:l
  %         orto(:,:,i)=ort(:,:,i)/(trace(ort(:,:,i)'*ort(:,:,i)));
   %        for j=i+1:l
    %         d(i,j)=trace(orto(:,:,i)'*ort(:,:,j));
     %          ort(:,:,j)=ort(:,:,j)-d(i,j)*orto(:,:,i);
      %     end
       %end
       %%


       % The second version of Gram-Schmidt algorithm
```

```
        ortoo=zeros(s,s,l);
orto=zeros(s,s,l);
ort=zeros(s,s,1);
ort=double(ort);
for i=1:s
   for j=1:s
      ort(i,j,1) = W(i,j,1);
   end
end

              for i=2:l

           for  j=1:i-1

d(i,j)=trace(W(:,:,i)'*ort(:,:,j))/(trace(ort(:,:,j)'*ort(:,:,j)));
                    orto(:,:,j)=d(i,j)*W(:,:,j);
                      ortoo(:,:,i)=orto(:,:,j)+ortoo(:,:,i);
                        end
            ort(:,:,i)=W(:,:,i)-ortoo(:,:,i);


                 end;




% calculation of the Zernike coefficients
                         co=eye(l,l);
           e=zeros(1,l);
        for i=1:l

e(1,i)=trace(phil0(:,:)'*ort(:,:,i))/(trace(ort(:,:,i)'*ort(:,:,i)));
                  end;
       '         e=double(e);
                 a=(inv(co+d))'*e';

                                  AL0=zeros(s,s,1);
                  We2=zeros(s,s,1);
                  We20=zeros(s,s,l);
                           for i=1:l
          We20(:,:,1)=a(i,1)*W(:,:,i);
       AL0(:,:,1)=AL0(:,:,1)+We20(:,:,1);
        end;
```

References

1) Handbook of Microlithography, Micromachining, and Microfabrication, vol. 1, edited by P. Roy Choudhury, *SPIE Optical Engineering Press*, (1999)

2) Donis G Flagello, Bernard Geh, "Lithographic lens testing: Analysis of measured aerial images", SPIE Vol. 2726, 788, (1996)

3) J. H. Bruning, J. E. Gallaghar, D. P. Rosenfeld, A.P. White, D. J. Brangaccio, and D. R. Herriot, "Digital Wavefront Interferometry for testing optical surfaces and lenses", Applied Optics, Vol. 13, 2693, (1974)

4) Norman Bobroff, Petra Fadi, " Bench evaluation of lithographic lenses from measurement of the point spread function", SPIE Vol. 922, 376, (1988)

5) Wolfgang Freitag, Wilfred Grossman, and Uwe Grunewald, "Aberration analysis in aerial images formed by lithographic lenses", Applied Optics, Vol. 31, No. 13, 2284, (1992)

6) Hiroshi Nomura, and Takashahi Sato, " Techniques for measuring aberrations in lenses used in photolithography with printed patterns", Applied Optics, Vol. 38, No. 13, (1999)

7) Optical Imaging and aberrations (ray geometrical optics), Vol. 1, Virendra Mahajan, *SPIE Optical Engineering Press*, (1998)

8) Aberration Theory Made Simple, Virendra Mahajan, *SPIE Optical Engineering Press*, (1992)

9) The Physics of Micro/Nano fabrication, Ivor Brodii, and Julius. J. Muray, *New York/Plenum Press*, (1992)

10) Fundamentals of Microelectronic Processing, Hong. H. Lee, *Mc Graw Hill*, (1990)

11) Donis. G. Flagello, Jorde Klerk, Guy Davies, Rich Pregoff, Bernard Geh, Michael Ari, Uli Wegmann, Michael Kraemer, " Towards a comprehensive control of full field image quality in optical photolithography", SPIE, Vol. 3051, 652, (1997)

12) T. A. Brunner, "Impact of lens aberrations on optical lithography", IBM Journal of Research and Development, Vol. 41, No. ½, (1997)

13) W.P. Linnik, Proc. Acad. Sci., USSR, 1, 208, (1933)

14) R. N. Smartt, and W. H. Steel, "Theory and application of Point Diffraction Interferometry", Jpn. J. of App. Physics, 14, Suppl. 14-1, 351, (1975)

15) H. Medeki, E. Tejnil, K. Goldberg, and J. Bokor, " Phase Shifting Point Diffraction Interferometry", Optics Letters, Vol. 21, No. 19, 1726, (1996)

16) K.A. Goldberg, E. Tejnil, S. H. Lee, H. Medecki, D. T. Atwood, K. H. Jackson, J. Bokor, " Phase Shifting Point Diffraction Interferometer", SPIE, Vol. 3048, 264, (1997)

17) E. Tejnil, K. A. Goldberg, H. Medecki, R. Beguirisain, J. Bokor, D. J. Atwood, "Phase Shifting Point Diffraction Interferometry for at wavelength testing of Lithographic Optics", OSA Tops on EUV, 118, (1996)

18) E.Tejnil, K.A. Goldberg, S. H. Lee, H. Medecki, P. J. batson, P. E. Denhabi, A. Mc Dowell, J. Bokor, and D. Atwood, " At wavelength interferometry for EUV", J. Vac. Sci. Tech. B, 15(6), (1996)

19) P. D. Nalleau, K. A. Goldberg, S. H. Lee, C. Cheng, P. Atwood, J. Bokor, " EUV PSPDI interferometer: a wavefront metrology tool with subangstrom reference wave accuracy", Applied Optics, Vol. 38, 35, 7252, (1999)

20) K. A. Goldberg, R. Beguiristin, J. Bokor, H. Medecki, K. Jackson, and D. T. Atwood, " Point diffraction Interferometry at EUV wavelength", OSA proceedings on EUV, (1994)

21) K.A. Goldberg, P. Nalleau, S. H. Lee, C. Bresloff, C. Henderson, D. Atwood, J. Bokor, " High accuracy interferometry of EUV lithography systems", J of Vac. Sci. Tech B, 16(6), 3435, (1998)

22) P. Nalleau, K. Goldberg, S. Lee, C. Cheng, C Bresloff, P. Batson, D. Atwood, J. Bokor, " Characterization of the accuracy of EUV PSPDI", SPIE, Vol. 3331, 114, (1998)

23) P. Nalleau, K. A. Goldberg, " Dual domain PDI", Applied optics, Vol. 38, 16, 3523, (1999)

24) K. A. Goldberg, P. Nalleau, J. Bokor, " EUV interferometric measurements of diffraction limited optics", J. Vac. Sci. Tech. B, 17(6), 2982, (1999)

25) Interferogram Analysis: Digital Fringe Pattern Measurement Technique, David, W. Robinson, and Greame. T. Reed, *Institute of Physics Publishing*, (1993)

26) Interferogram Analysis for Optical Shop Testing, Daniel Malacara, Manuel Servin, Zacharias Malacara, *Marcel Dekker Inc,* (1999)

27) Optical Shop Testing, edited by Daniel Malacara, *John Wiley and sons Inc,* (1992)

28) David J Fisher, John T O' Bryan, Robert Lopez, H Philip Stahl, " Vector formulation for interferogram surface fitting", Applied Optics, Vol. 32(25), (1993)

29) Takeda M, Ina. H. and Kobayashi. S, JOSA, 72, 156, (1982)

30) Microlithography, Science and Technology, edited by James R. Sheats, and Bruce W. Smith, *Marcel Dekker Inc,* (2000)

31) Joseph E. Gortych, and David Williamson, "Effects of Higher Order Aberrations on the Process Window", SPIE, vol. 1463, 368, (1991)

32) The Art and Science of Optical Design, Shannon R R, *Cambridge University Press*, (1997)

33) www.litel.net